

Earth's Future

RESEARCH ARTICLE

10.1029/2023EF003977

Key Points:

- Structural overshoot accounted for over 1/3 drought events in Northwest China drylands during 1982–2015
- Nearly 20% vegetation declines were caused by vegetation lagged effects of overshoot droughts
- Structural overshoot drought frequency increased due to vegetation overgrowth trailed by precipitation

Supporting Information:

Supporting Information may be found in the online version of this article.

Correspondence to:

L. Liu,
liuliu@cau.edu.cn

Citation:

Zhang, Y., Liu, L., Cheng, Y., Kang, S., Li, H., Wang, L., et al. (2024). Intensified structural overshoot aggravates drought impacts on dryland ecosystems. *Earth's Future*, 12, e2023EF003977. <https://doi.org/10.1029/2023EF003977>






Received 1 SEP 2023
Accepted 20 DEC 2023

Author Contributions:

Conceptualization: Liu Liu, Shaozhong Kang
Data curation: Yixuan Zhang, Yongming Cheng, Yu Shi
Formal analysis: Yixuan Zhang, Liu Liu
Investigation: Yixuan Zhang, Liu Liu, Yongming Cheng
Methodology: Yixuan Zhang, Liu Liu, Yongming Cheng
Resources: Liu Liu, Shaozhong Kang
Software: Yixuan Zhang, Yongming Cheng
Supervision: Liu Liu, Shaozhong Kang
Validation: Yixuan Zhang, Liu Liu
Writing – original draft: Yixuan Zhang, Liu Liu, Yongming Cheng

© 2024 The Authors. Earth's Future published by Wiley Periodicals LLC on behalf of American Geophysical Union. This is an open access article under the terms of the [Creative Commons Attribution License](https://creativecommons.org/licenses/by/4.0/), which permits use, distribution and reproduction in any medium, provided the original work is properly cited.

Intensified Structural Overshoot Aggravates Drought Impacts on Dryland Ecosystems

Yixuan Zhang^{1,2}, Liu Liu^{1,2} , Yongming Cheng^{1,2}, Shaozhong Kang^{1,2} , Hao Li³ , Lixin Wang⁴ , Yu Shi^{1,2}, Xingcai Liu⁵ , and Lei Cheng⁶

¹State Key Laboratory of Efficient Utilization of Agricultural Water Resources, China Agricultural University, Beijing, China, ²Center for Agricultural Water Research in China, China Agricultural University, Beijing, China, ³Hydro-Climate Extremes Lab, Ghent University, Ghent, Belgium, ⁴Department of Earth and Environmental Sciences, Indiana University Indianapolis, Indianapolis, IN, USA, ⁵Institute of Geographic Sciences and Natural Resources Research, Chinese Academy of Sciences, Beijing, China, ⁶State Key Laboratory of Water Resources and Hydropower Engineering Science, Wuhan University, Wuhan, China

Abstract A favorable environment can induce vegetation overgrowth to exceed the ecosystem carrying capacity, exacerbating water resource depletion and increasing the risk of lagged effects on vegetation degradation. This phenomenon is defined as structural overshoot, which can lead to large-scale forest mortality and grassland deterioration. However, the current understanding of structural overshoot remains incomplete due to the complex time-varying interactions between vegetation and climate. Here, we used a dynamic learning algorithm to decompose the contributions of vegetation and climate to drought occurrence, trace the connection between antecedent and concurrent vegetation dynamics, thus effectively capturing structural overshoot. This study focused on the climate-sensitive hotspot in Northwest China drylands, where significant vegetation greening induced by a warming and wetting climate was detected during 1982–2015, leading to soil moisture deficit and aggravating vegetation degradation risks during droughts. We found that during this period, structural overshoot induced approximately 34.6% of the drought events, and lagged effects accounted for 16.7% of the vegetation degradation for these overshoot drought events. The occurrence of overshoot droughts exhibited an increasing trend over time, which was primarily driven by vegetation overgrowth followed by precipitation variation. Although the severity of overshoot and non-overshoot droughts were generally comparable in spatial distribution, the impact of overshoot droughts is still becoming increasingly obvious. Our results indicate that the expected intensified overshoot droughts cannot be ignored and emphasize the necessity of sustainable agroecosystem management strategies.

Plain Language Summary Structural overshoot droughts, defined as the vegetation growth that exceeds the ecosystem carrying capacity due to the favorable environments, have posed substantial threats to Northwest China drylands. Using a dynamic learning algorithm driven by satellite and reanalysis data, we conducted comprehensive assessments of the impact of structural overshoot on drought occurrence in the dryland ecosystem of Northwest China. Our results reveal that structural overshoot accounted for over one-third of drought events, and demonstrated increasing trends from 1982 to 2015. The frequency and impact of structural overshoot droughts are expected to increase in a warming climate, which highlights the importance of sustainable land use management.

1. Introduction

Drought causes significant damage to the natural environment and human society by reducing the availability of water resources (Buermann et al., 2018; Jiao et al., 2021; Rodell et al., 2018). Numerous studies have documented the trends of drought under climate change (Dai, 2013; Samaniego et al., 2018; Williams et al., 2020), whereas few studies have paid attention on the vegetation overgrowth to a favorable environment, which will exacerbate the impacts of drought on dryland ecosystems (Lian et al., 2021). A complex relationship exists between climate systems and ecosystems. The state of ecosystems is influenced not only by the concurrent climate status but also by the preceding climate conditions (Bastos et al., 2020; Wolf et al., 2016). In boreal ecosystems, warmer springs can drive an earlier onset of the growing season (Piao et al., 2015), which may enhance evapotranspiration (ET) (Kang et al., 2006), resulting in further depletion of soil moisture (SM) and triggering of seasonal SM deficit (Buermann et al., 2013; Lian et al., 2020), eventually leading to negative lagged effects on ecosystem functions

Writing – review & editing: Yixuan Zhang, Liu Liu, Shaozhong Kang, Hao Li, Lixin Wang, Xingcai Liu, Lei Cheng

in the summer or even autumn (Buermann et al., 2018; Richardson et al., 2010). This phenomenon, defined as structural overshoot, often occurs in regions with extensive forest cover (S. Wang et al., 2020). It can elicit more severe threats to grasslands and agricultural lands because their relatively shallow roots prevent them from accessing deep SM (Bastos et al., 2020).

Several studies documented drought related to structural overshoot. Such as the unusual drought and heat stricken central and northern Europe in the summer 2018, which was detected by Bastos et al. (2020) as the legacy of water deficit dominance, which extremely amplified drought impacts on crop harvests and carbon fluxes. Similarly, Wolf et al. (2016) documented water limitations due to the warmer spring induced biological atmospheric feedback in America 2012 summer drought, however, earlier vegetative activity to some extent compensated for carbon storage decline during the summer drought. An implication could be drawn from Jiao et al. (2022) that lagged drought may have more significant effects compared to simultaneous drought. Compared to cumulative atmospheric deficit effects on vegetation productivity (Z. Zhang et al., 2022), the legacy negative SM limitation induced by vegetative growth would be more informative for comprehending the mechanisms and effects of overshoot (Goulden & Bales, 2019), especially in water-limited drylands. In addition, some of the recent studies mainly focused on the vegetation phenology in the background of changing seasonal characteristics and legacy effects of previous droughts, and addressed the legacy negative effects on vegetation growth caused by an earlier start of spring phenology (Mei et al., 2021; Zeng et al., 2021). However, due to the complex time-varying interactions between vegetation, climate and human activities, there is an incomplete understanding of structural overshoot induced drought, which hinders the development of adaptive strategies to cope with the anticipated intensification of drought frequency, duration, and severity (Jump et al., 2017). Climate change regulates vegetation phenology and alters ecosystem functions (Piao et al., 2015; L. Wang, 2023; C. Wu et al., 2022), which in turn affects the environment through vegetation biogeochemical and biophysical processes (Peñuelas et al., 2009). Therefore, a comprehensive assessment of the interaction mechanisms between vegetation dynamics and drought evolution is conducive to our understanding of regional water and carbon cycles, as well as ecosystem responses and feedback to climate change (Y. Liu et al., 2022).

Structural overshoot has already been detected in forest ecosystems, revealing one of the reasons for previous sharp declines in the forest (Jump et al., 2017). Incorporating in-site and remote sensing observations, Goulden and Bales (2019) explored the mechanisms of marked tree mortality in California's 2012–2015 drought, and illuminated the links between tree die-off and cumulative deep-soil drying. Furthermore, Y. Zhang et al. (2021) quantified the spatial patterns and impacts of structural overshoot at a global scale, and further defined its concept as vegetation overgrowth induced by prior favorable climatic conditions that could temporarily exceed the carrying capacity of the ecosystem, potentially depleting SM resources in the process. Negative lagged effects caused by structural overshoot may increase the risk of future droughts, as well as amplify the impact of climate change (Goulden & Bales, 2019). However, in the study conducted by Y. Zhang et al. (2021), radiation was not considered as the major influencing factor that plays an important role in the growth of vegetation in drylands (H. Wang et al., 2022), and there is a lack of studies on the structural overshoot in water-limited drylands, which occupy over 40% area of the global land (L. Wang et al., 2022). Given the significant regional discrepancies in spatiotemporal characteristics, the response and feedback mechanisms of vegetation to climate vary considerably at different timescales across regions. Therefore, it is essential to conduct an in-depth investigation of the relationship between regional vegetation dynamics and drought evolution, especially the contribution of structural overshoot to subsequent drought events and its impacts on dryland ecosystems.

The typical arid inland region of Northwest China (NWC) is located in the mid-latitudes of Eurasia. With scarce water resources year-round, NWC is one of the most vulnerable regions to global climate change (Chen et al., 2015). As an important ecological security barrier in arid regions, vegetation plays a crucial role in wind and sand control in NWC (Cao et al., 2021). Vegetation in NWC has experienced significant upward trends owing to the modulations caused by the climate transition from warm-dry to warm-wet (Jiapaer et al., 2015; Q. Zhang et al., 2021), which concurs with mass water consumption. The climate is projected to continue warming and humidification in NWC (Q. Zhang et al., 2022), creating an ideal environment for vegetation to flourish. However, enhanced vegetation growth or an earlier start of the growing season could exacerbate the risk of structural overshoot, intensify water scarcity, and eventually leave profound negative legacy effects on vegetation growth in the subsequent growing season (Zeng et al., 2021). This series of events caused by climate change and increasing human activities could be detrimental to the development of ecosystem service functions in NWC (Lai et al., 2022; Sun et al., 2006; Wei et al., 2022; Zeng et al., 2021). Much of the existing research has focused on

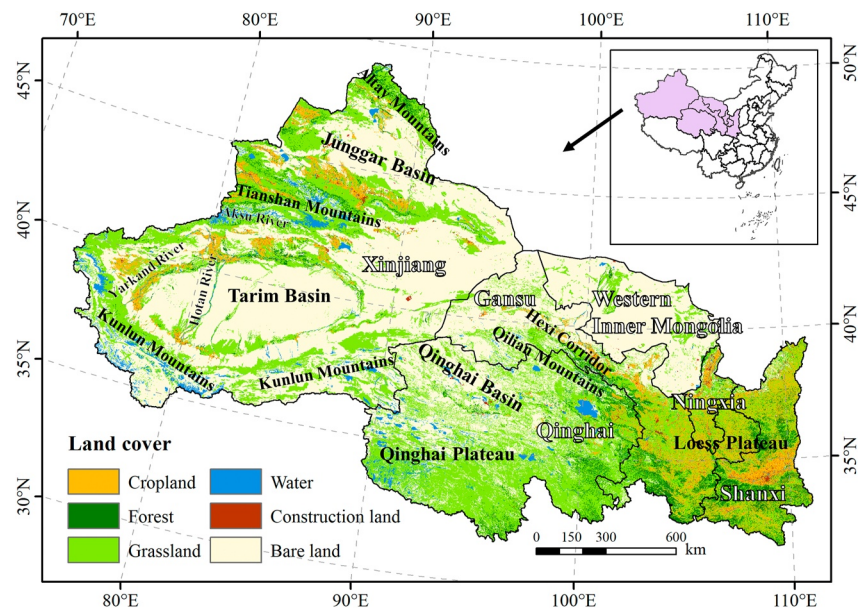


Figure 1. The spatial distribution of land cover types in Northwest China in the year 2015. Note: The land cover data were derived from <http://www.resdc.cn>, <https://doi.org/10.12078/2018070201>. A detailed demonstration of the spatial distribution of NDVI, air temperature, precipitation, and downward longwave radiation (DLR) averaged across 1982–2015 can be seen in Figure S1 of the Supporting Information S1.

the response of vegetation to climate change (Cao et al., 2021, 2022; Chen et al., 2015, 2020; Z. Du et al., 2017; Jiapaer et al., 2015; Mo et al., 2019); however, less attention has been devoted to vegetation feedback owing to the complexity of dynamic vegetation-climate interactions. Thus, as a climate change hotspot, effective identification of the structural overshoot in the context of warming and humidification in NWC has become essential for alleviating the contradiction between water supply and demand. In particular, it is of great significance for maintaining optimal ecosystem service functions both in China and globally.

In this study, a Bayesian Dynamic Linear Model (DLM) (West & Harrison, 2006), including a sensitivity coefficient that can vary over time to capture non-linear vegetation variations, is proposed to identify overshoot induced drought. The analyses are based on the combination of the Standardized Precipitation Evapotranspiration Index (SPEI) and Normalized Difference Vegetation Index (NDVI), which represent drought conditions and vegetation greenness (Y. Zhang et al., 2021), respectively. The main objectives of this study were to (a) quantify drought events triggered by structural overshoot, (b) examine the potential driving mechanisms of the structural overshoot phenomenon, and (c) characterize the impacts of overshoot induced droughts in NWC. Our findings are expected to provide the practical foundation for formulating effective land management strategies and promoting long-term regional ecosystem sustainability.

2. Materials and Methods

2.1. Study Area

Northwest China (73°46′–111°25′E, 31°58′–49°19′N) includes the provinces of Qinghai, Gansu, and Shanxi, as well as the Xinjiang Uygur Autonomous Region, the Ningxia Hui Autonomous Region, and the western part of Inner Mongolia (Figure 1). The complex mountainous terrain hinders the transportation of moist air from the ocean, forming a primary temperate continental climate, with precipitation gradually decreasing from southeast to northwest. In most areas of NWC, the annual mean precipitation is below 400 mm, with less than 100 mm in southern Xinjiang. Apart from that, southern Shanxi, exceeds 400 mm, with certain areas experiencing precipitation of up to 800 mm per year (Figure S1c in Supporting Information S1). As a result of global warming, the climate pattern in NWC has recently shifted from warm-dry to warm-wet, and precipitation has been noticeably increasing (Jiapaer et al., 2015). This pattern, together with the abundance of sunshine duration, provides an ideal condition for vegetation growth. A variety of vegetation and soil types can be observed in this region, with grassland and desert being the two predominant types of land cover (Figure 1). Human activities have

significantly increased the irrigated land in Xinjiang and the Hexi Corridor, and large-scale ecological restoration initiatives, such as the “Grain for Green Project” on the Loess Plateau and the “Three-North Shelter Forestation Project” in Inner Mongolia, have also stimulated the vegetation in these areas to experience a remarkable greening trend. Overall, this series of changes emphasizes the urgency and importance of examining the structural overshoot of vegetation in NWC.

2.2. Data Sets

2.2.1. Vegetation Index

NDVI is a widely used proxy for monitoring and quantifying changes in vegetation growth and can reflect vegetation biomass and phenology (Tucker et al., 1986). The third-generation NDVI (NDVI3g) data set released by the Global Inventory Modeling and Mapping Studies Project (GIMMS) of the National Aeronautics and Space Administration (NASA) (Pinzon & Tucker, 2014) was used in this study. The GIMMS NDVI3g data products comprised a global data set with a spatial resolution of $1/12^\circ$ (8 km at the equator) and a temporal resolution of 15-day intervals, with the longest time series available from July 1981 to December 2015. This data set has been verified to have the best temporal consistency (Marshall et al., 2016) and has been extensively used in China (Liang & Yang, 2016; Tao et al., 2017; H. Wang et al., 2022; H. J. Xu et al., 2018). Data from 1982 to 2015 were extracted in this study, and to further reduce the impact of clouds and haze, monthly values were integrated using the Maximum Value Composite (MVC) technique (Holben, 1986). Meanwhile, to exclude the effects of non-vegetation areas, areas with a mean NDVI value of less than 0.1 were omitted (Jamali et al., 2014).

We added data sets of kernel NDVI (kNDVI) and Solar-induced Chlorophyll Fluorescence (SIF) to evaluate the results obtained by NDVI (Jeong et al., 2017; W. Li et al., 2022). kNDVI proposed by Camps-Valls et al. (2021) has the advantage of improving the optical signal saturation impacts of NDVI. SIF provides a more rapid and precise method to evaluate the status of vegetation based on the light signal generated by vegetation photosynthesis (Sun et al., 2023) and serves as an effective proxy for GPP (Yang et al., 2015). A global contiguous SIF (CSIF) (Y. Zhang et al., 2018) all-sky daily average data set that has high spatiotemporal resolutions and reliability generated using neural networks was used from 2001 to 2015.

2.2.2. Climate Data

Climate data were obtained from the China Meteorological Forcing Dataset (CMFD) (He et al., 2020). The CMFD is a reanalysis data product that combines information from traditional meteorological stations, radar, and remote sensing, spanning the years 1979–2018 with a temporal resolution of 3 hr and a spatial resolution of 0.1° . The reliability and applicability of the CMFD data set have been extensively investigated (B. L. Xue et al., 2013; Yang et al., 2021) and compared with in situ observations in arid and semi-arid regions (Chen et al., 2011). The mean air temperature, precipitation, downward longwave radiation (DLR), and specific humidity were chosen from the seven meteorological factors provided in the CMFD data set (Nemani et al., 2003; Rishmawi et al., 2016; Tao et al., 2017; D. Wu et al., 2015).

Additionally, vapor pressure deficit (VPD) was extracted from the data set of the TerraClimate (Abatzoglou et al., 2018), spanning from 1982 to 2015 with monthly temporal resolution and a $1/24^\circ$ spatial resolution.

2.2.3. Soil Moisture Data

ERA5 is the fifth-generation global climate reanalysis data set released by the European Center for Medium-Range Weather Forecasts (ECMWF). The ERA5-Land data set was generated by replaying the land surface component of ERA5 and had higher spatiotemporal resolutions (Hersbach et al., 2020). With $0.1^\circ \times 0.1^\circ$ grid spacing and hourly temporal resolution from 1950 to the present, ERA5-Land contains detailed records of SM content for four soil layers (0–7, 7–28, 28–100, and 100–289 cm). Given that the 0–100 cm soil depth accounts for the majority of vegetation roots (A. Wang & Kong, 2021), the values in the top three soil layers were extracted in this study, and monthly SM data were generated by weighted interpolation. Based on this, the Soil Water Deficit Index (SWDI) (Martínez-Fernández et al., 2015) was calculated to serve as a foundation for the Random Forest (RF) model to investigate the underlying mechanisms of structural overshoot.

2.2.4. Climatological Drought Index

SPEI (Vicente-Serrano et al., 2010) characterizes the long-term water balance by calculating the difference between precipitation and potential evapotranspiration, which has been widely used to evaluate drought conditions

(Cao et al., 2021; C. Wu et al., 2022; H. J. Xu et al., 2018). The monthly SPEI data products employed in this study at different timescales ranging from 1 to 48 months were calculated based on the Climatic Research Unit (CRU) meteorological data, with a spatial resolution of 0.5° . Considering that vegetation productivity responds significantly to the 3-month timescale of the SPEI (SPEI-3) in arid regions (Zhao et al., 2018), the SPEI-3 data set was used in this study to reflect seasonal moisture deficits.

To ensure consistent spatial resolution across different data sets, all variables were interpolated to grid cells with a resolution of $0.5^\circ \times 0.5^\circ$ using the bilinear interpolation algorithm.

2.3. Methods

2.3.1. Trend Analysis

The least-squares linear regression model was used to investigate the trends in NDVI, meteorological factors (i.e., temperature, precipitation, and DLR), and SM at the pixel scale from 1982 to 2015 using the following equation (Jiapaer et al., 2015; Zheng et al., 2021):

$$\text{Slope} = \frac{n \sum_{i=1}^n (i \times x_i) - \sum_{i=1}^n i \sum_{i=1}^n x_i}{n \sum_{i=1}^n i^2 - (\sum_{i=1}^n i)^2} \quad (1)$$

where Slope represents a linear trend, n is the number of time series ($n = 34$), and x_i is the value of each factor in the year i . Slope > 0 indicates a positive trend and Slope < 0 indicates a negative trend of the variable over time. The t -test was used at a significance level of 0.05.

2.3.2. Correlation Analysis

The Pearson correlation coefficient was used to examine the response of NDVI to each meteorological factor (i.e., temperature, precipitation, and DLR) and its correlation with SM, based on the following formula (Mo et al., 2019; Wei et al., 2022):

$$r_{xy} = \frac{\sum_{i=1}^n (x_i - \bar{x})(y_i - \bar{y})}{\sqrt{\sum_{i=1}^n (x_i - \bar{x})^2 \sum_{i=1}^n (y_i - \bar{y})^2}} \quad (2)$$

where r_{xy} is the correlation coefficient between NDVI and other variables, n is the number of time series ($n = 34$), x_i is the value of NDVI in the year i , y_i is the value of each meteorological factor or SM in the year i , and \bar{x} and \bar{y} are the mean values of x and y , respectively. $r_{xy} > 0$ indicates a positive correlation and $r_{xy} < 0$ indicates a negative correlation between NDVI and each other variable. A larger absolute value of r_{xy} indicates a stronger correlation between the two variables. The t -test was used at a significance level of 0.05.

2.3.3. Bayesian Dynamic Linear Model

The Bayesian DLM (West & Harrison, 2006) is a linear model for time-series analysis, and because of its varied regression coefficients over time, it is possible to effectively capture the connection of vegetation conditions at different timescales. In this study, the model was developed based on Y. Zhang et al. (2021) and Y. Liu et al. (2019), which focused on the lagged effects of previous vegetation anomalies and concurrent climate anomalies. The DLM is composed of an observation equation (Equation 3) and a state evolution equation (Equation 4):

$$y_t = \mathbf{F}_t^T \boldsymbol{\theta}_t + v_t \quad (3)$$

$$\boldsymbol{\theta}_t = \mathbf{G} \boldsymbol{\theta}_{t-1} + \mathbf{w}_t \quad (4)$$

where y_t is the value of NDVI observation at each time t , which is decomposed by the model into three components: the local mean and trend component (subscript l), the seasonal component (subscript s), and the regression component (subscript r). The regression vector (\mathbf{F}_t), the state vector ($\boldsymbol{\theta}_t$, i.e., the sensitivity coefficient of DLM), and the state evolution matrix (\mathbf{G}) are also composed of the three corresponding components. v_t is the observation noise at the time t , following a Gaussian distribution with a zero mean; and \mathbf{w}_t is the state evolution noise at the time t , following a Gaussian distribution with a zero mean, which is independent of v_t .

$$\mathbf{F}_t = \begin{bmatrix} \mathbf{F}_l \\ \mathbf{F}_s \\ \mathbf{F}_{r,t} \end{bmatrix}, \boldsymbol{\theta}_t = \begin{bmatrix} \theta_{l,t} \\ \boldsymbol{\theta}_{s,t} \\ \boldsymbol{\theta}_{r,t} \end{bmatrix}, \mathbf{G} = \begin{bmatrix} \mathbf{G}_l & 0 & 0 \\ 0 & \mathbf{G}_s & 0 \\ 0 & 0 & \mathbf{G}_r \end{bmatrix} \quad (5)$$

- (1) The local mean and trend component of NDVI including:

$$\mathbf{F}_l = \begin{bmatrix} 1 \\ 0 \end{bmatrix}, \theta_{l,t} = \begin{bmatrix} \theta_{l1,t} \\ \theta_{l2,t} \end{bmatrix}, \mathbf{G}_l = \begin{bmatrix} 1 & 1 \\ 0 & 1 \end{bmatrix}$$

where $\theta_{l1,t}$ and $\theta_{l2,t}$ indicate the local mean and trend of NDVI in the time t , respectively.

- (2) The seasonal component includes three Fourier forms of seasonality frequencies at $\omega_1 = \frac{\pi}{6}, \omega_2 = \frac{\pi}{3}, \omega_3 = \frac{2\pi}{3}$:

$$\mathbf{F}_s = \begin{bmatrix} \mathbf{F}_{s1} \\ \mathbf{F}_{s2} \\ \mathbf{F}_{s3} \end{bmatrix}, \boldsymbol{\theta}_{s,t} = \begin{bmatrix} \theta_{s1,t} \\ \theta_{s2,t} \\ \theta_{s3,t} \end{bmatrix}, \mathbf{G}_s = \begin{bmatrix} \mathbf{G}_{s1} & 0 & 0 \\ 0 & \mathbf{G}_{s2} & 0 \\ 0 & 0 & \mathbf{G}_{s3} \end{bmatrix}$$

where

$$\mathbf{F}_{si} = \begin{bmatrix} 1 \\ 0 \end{bmatrix}, \theta_{si,t} = \begin{bmatrix} \theta_{si,1,t} \\ \theta_{si,2,t} \end{bmatrix}, \mathbf{G}_{si} = \begin{bmatrix} \cos \omega_i & \sin \omega_i \\ -\sin \omega_i & \cos \omega_i \end{bmatrix}, i \in \{1, 2, 3\}$$

- (3) The regression component consists of:

$$\mathbf{F}_{r,t} = [x_{1,t}, x_{2,t}, \dots, x_{p,t}]^T, \boldsymbol{\theta}_{r,t} = [\theta_{r,1,t}, \theta_{r,2,t}, \dots, \theta_{r,p,t}]^T, \mathbf{G}_r = \mathbf{I}_p$$

where \mathbf{I}_p is the identity matrix with a dimension of p . In the regression components of $\mathbf{F}_{r,t}$, each variable represents concurrent temperature anomalies (δTemp), precipitation anomalies from concurrent and previous 2 months ($\delta\text{Prec}_{t,t-2}$), concurrent radiation anomalies (δDLR_t), NDVI anomalies with 1 month lag (δNDVI_{t-1}), NDVI anomalies with a 2–3 months lag ($\delta\text{NDVI}_{t-2,t-3}$), NDVI anomalies with a 4–6 months lag ($\delta\text{NDVI}_{t-4,t-6}$), NDVI anomalies with a 7–12 months lag ($\delta\text{NDVI}_{t-7,t-12}$), and NDVI anomalies with a 13–24 months lag ($\delta\text{NDVI}_{t-13,t-24}$). The mean value between the starting and ending months was calculated based on the subscripts of each variable. NDVI with 1 month lag (lag 1) was considered as a direct effect in this study owing to its significant autocorrelation and is often considered as an indicator of intrinsic vegetation memory or used to indicate the vegetation recovery rate (Kusch et al., 2022). Similarly, $\boldsymbol{\theta}_{r,t}$ also consists of the coefficient corresponding to $\mathbf{F}_{r,t}$ that represents the influence of previous NDVI components or climate factors.

At each time t , starting with the provided non-informative priors of $\boldsymbol{\theta}_0$ and noises, the posterior distribution of $\boldsymbol{\theta}_t$ is estimated using a forward filtering approach. In addition, to obtain a more reliable prediction of the coefficient, the first 5 years (1982–1987) of both satellite-observed NDVI and precipitation (10 years in total) were recycled twice before the start of the prediction.

2.3.4. Identification of Droughts and Overshoot Droughts

In this study, both SPEI and NDVI were utilized to characterize drought. Figure 2 shows the identification of overshoot induced drought during 2002–2003 and serves as an example of the theory, procedure, and results of the DLM approach. First, NDVI anomalies (Figure 2b) were obtained from the long-term NDVI observations (Figure 2a). The DLM decomposed the NDVI time series into three separate components: a local mean and trend component, three seasonal components, and a deseasonalized detrended regression component (Figure 2c). Second, the possible drought period was defined as the beginning when the deseasonalized detrended NDVI anomaly turned negative and terminated when the deseasonalized detrended NDVI anomaly was more than 70%

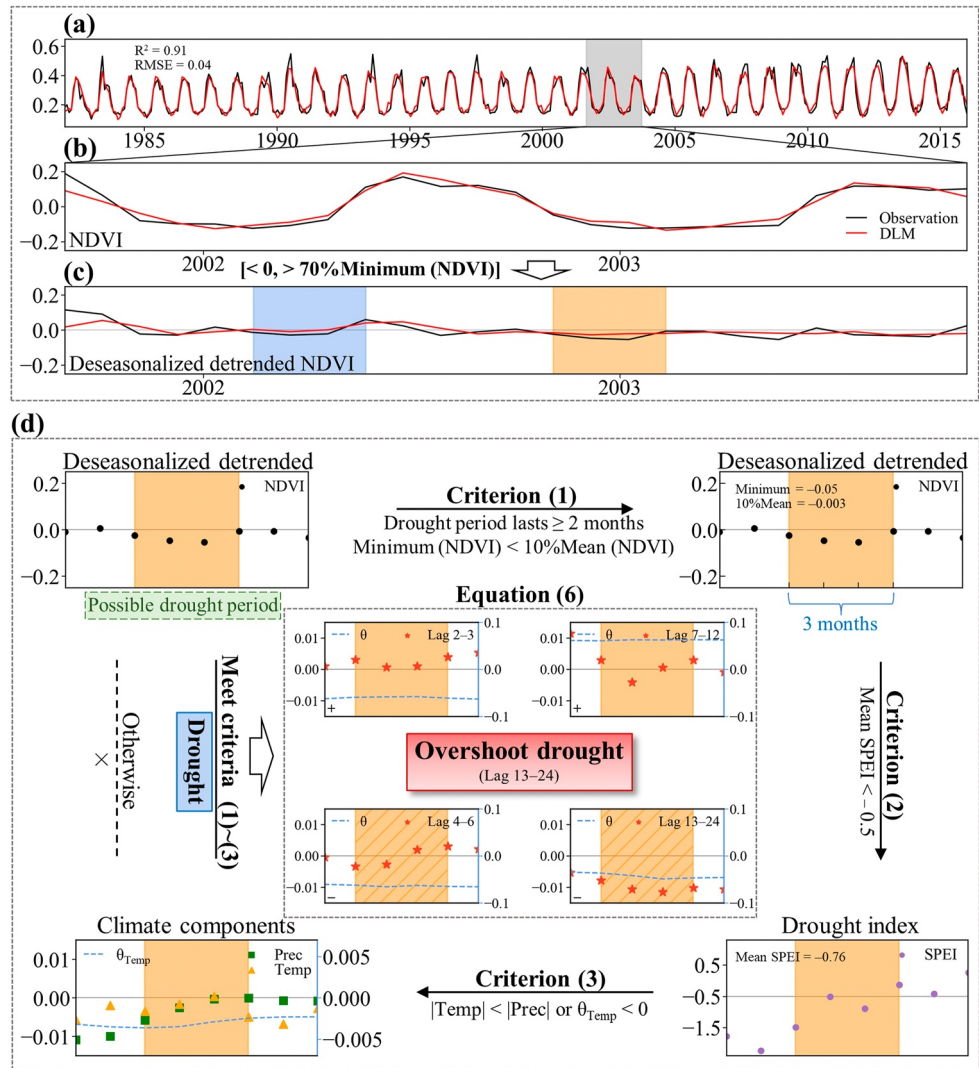


Figure 2. An example of overshoot drought identified using the DLM in NWC (103.96°E, 35.96°N). (a) NDVI time series from satellite observations (black), and DLM predictions (red) from 1982 to 2015. (b) NDVI anomalies (NDVI values minus multi-year averages). (c) Deseasonalized detrended NDVI (the black line indicates NDVI anomalies minus trend and seasonal components, and the red line indicates DLM predictions, calculated by summing the components of precipitation, temperature, DLR, and all lagged NDVI). (d) Flowchart of overshoot drought identification. Starting with the possible drought period, three criteria are examined to confirm the drought event, following which overshoot drought is identified. The blue-shaded and orange-shaded areas both represent the confirmed drought period; however, only the orange-shaded area is eventually identified as an overshoot drought period and is used for further explanation, with hatches indicating the overshoot components. The blue dashed lines represent the sensitivity coefficient corresponding to each variable (right axis).

of its minimum value. On this basis, a drought event (as shown in Figure 2d) was recognized when the following three criteria were met: (a) the drought period lasts at least 2 months and the minimum deseasonalized detrended NDVI anomaly should be less than 10% of its mean value to exclude the effect of random noise in NDVI; (b) the mean SPEI during the corresponding period is less than -0.5 ; (c) the absolute value of the temperature component should be smaller than that of the precipitation component during the drought period, or the temperature sensitivity coefficient should be negative, to exclude the disturbance of NDVI declines due to low temperature instead of low SM.

Based on the identification results of drought events, four different lagged timescales of NDVI were assessed to identify droughts triggered by structural overshoot (i.e., overshoot droughts): a 2–3 months lag (lag 2–3, i.e., sub-seasonal), 4–6 months lag (lag 4–6, i.e., seasonal), 7–12 months lag (lag 7–12, i.e., intra-annual), and 13–24 months lag

(lag 13–24, i.e., inter-annual). The average lagged NDVI anomalies ($\mathbf{F}_{r,i} = [x_{2-3}, x_{4-6}, x_{7-12}, x_{13-24}]^T$) and corresponding DLM sensitivities ($\theta_{r,i}$) were first calculated. For each timescale, if $x_i > 0$ and $\theta_{r,i} < 0$ ($i \in \{2-3, 4-6, 7-12, 13-24\}$), which means the lagged NDVI contributed to the concurrent prediction $\text{contri}_i = x_i * \theta_{r,i} < 0$, then this contri_i was regarded as an overshoot component (overshoot_contri), whereas the remaining components were seen as non-overshoot components (non-overshoot_contri). For each drought event, if Equation 6 is satisfied,

$$|\text{sum(overshoot_contri)}| > |\text{sum(non-overshoot_contri)}| \quad (6)$$

which indicates that there was a structural overshoot brought on by the previous excessive NDVI increase, which harms concurrent vegetation dynamics. Consequently, this drought event was identified as an overshoot drought event (Figure 2d). Besides, the SM time-series before and during the overshoot drought event was shown to demonstrate the mechanism of structural overshoot (see Figure S2 in Supporting Information S1 for details).

When there was more than one overshoot component, we further defined an overshoot drought event caused by the timescale at which the overshoot component with the greatest negative contribution is located (as shown in Figure 2d, the overshoot drought observed in 2002–2003 was caused by the inter-annual timescale (lag 13–24) because the negative contribution of the overshoot component in the previous 13–24 months was greater than that in the previous 4–6 months). In addition, the effects of overshoot drought on vegetation were characterized using deseasonalized detrended NDVI anomalies.

2.3.5. Random Forest Model

RF is a machine learning algorithm introduced by Breiman (2001), which has been widely used in various scientific fields such as geography and remote sensing (Belgiu & Drăguț, 2016; Shruthi et al., 2014). RF consists of multiple decision trees with the same distribution, which are independently based on the values of bootstrapped samples. After selecting random features for each node, the nodes are split, and the prediction results are determined by a plurality vote of the tree predictors. The classification model used in this study consisted of 400 trees, with a minimum sample size of eight for node split and leaf node samples no smaller than three. The model was developed using 70% of the entire data set and included six possible factors (temperature, precipitation, DLR, NDVI, SPEI, and SWDI) to predict whether an overshoot drought event had occurred. Thereafter, the internal out-of-bag error estimation was calculated using approximately one-third portion of the data that was randomly excluded from the constructed 400 classification trees (Lawrence et al., 2006). Moreover, to adequately validate the performance of our model, a confusion matrix was used to calculate the overall accuracy of the predictions using test data set that was previously withheld (30% of the entire data set). With the optimal fitted model, the variable importance (VI) was estimated as a decrease in the Gini coefficient of node splitting. Higher VI values indicated that the variable was more important.

The partial dependence plot (PDP) (Friedman, 2001) reflects the average marginal effect of each independent variable on the prediction target by fixing the value of the variable of interest and computing the average values of prediction obtained by changing other features using the following equation:

$$\hat{f}_s(x_s) = \frac{1}{n} \sum_{i=1}^n \hat{f}(x_s, x_c^{(i)}) \quad (7)$$

where \hat{f}_s is the partial dependence function corresponds to the interested variable x_s , x_c is the vector comprised of the other variables used in the RF model, with the superscript “(i)” representing one instance in the data set, and n is the number of incidents.

3. Results

3.1. Spatiotemporal Variations of Climate Factors and Vegetation

During 1982–2015, 80% of the vegetated areas in NWC exhibited a significantly increasing trend in temperature (Figure 3a), with a small fluctuation along latitude (Figure 3g). Meanwhile, the percentage of increase and the remarkable increase in precipitation of vegetated areas was 89.1% and 48.6%, respectively, whereas only 10.9% of the vegetated areas exhibited a slight downward trend, mostly distributed in southern Gansu and southeastern Shaanxi (Figure 3b). Furthermore, approximately 70.9% of the pixels showed a significantly increasing trend in

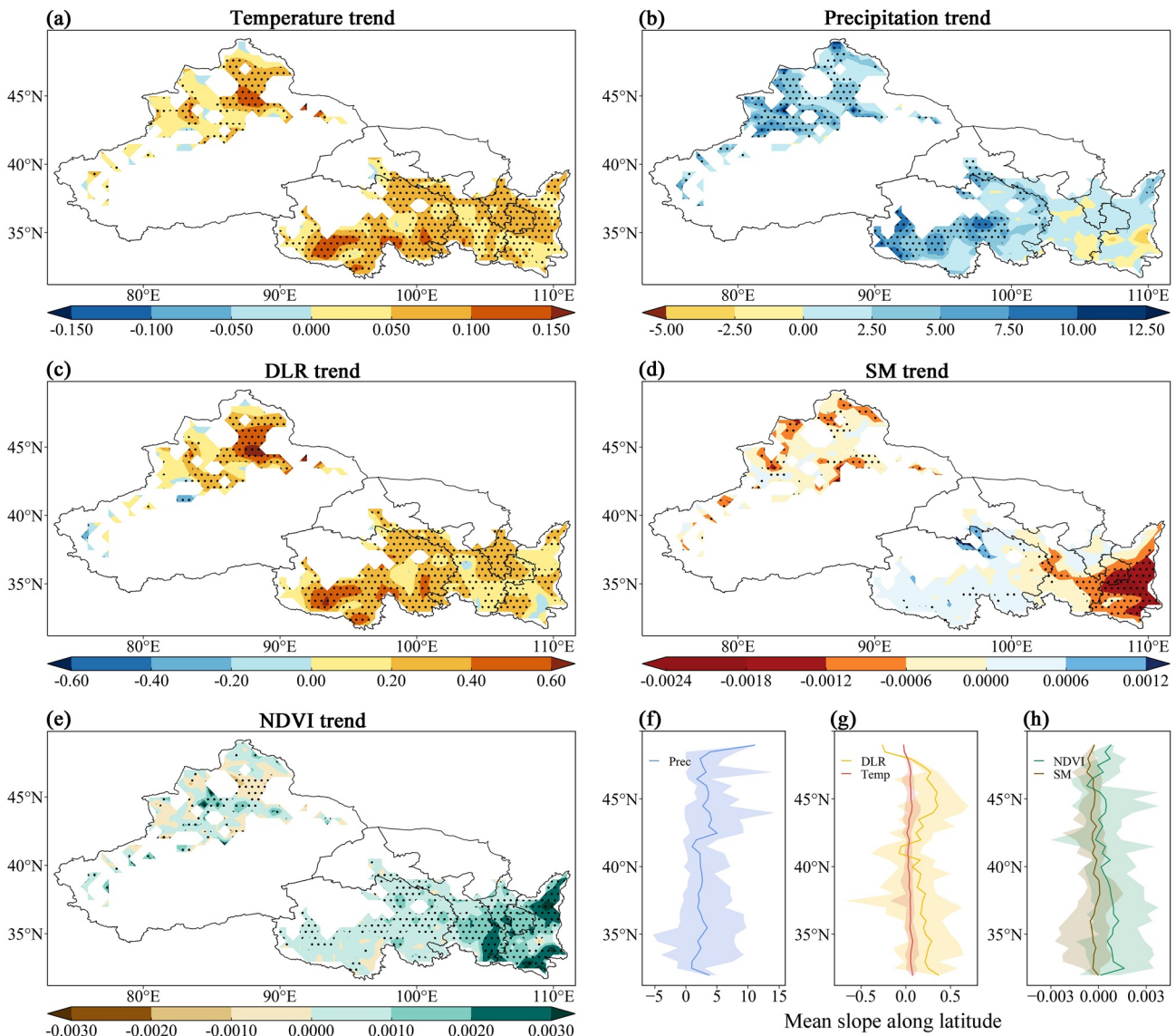


Figure 3. Spatial distributions of linear trends in (a) annual mean temperature, (b) annual precipitation, (c) annual mean DLR, (d) annual mean SM, and (e) annual mean NDVI, and the mean linear trends along the same latitude in (f) Precipitation–precipitation, (g) DLR and Temp–temperature, and (h) NDVI and SM. Shaded areas represent the maximum to minimum values at the same latitude. Black dots indicate statistically significant trends ($p < 0.05$).

DLR; in comparison, only a small proportion (29.1%) exhibited a slightly decreasing trend, mostly appearing in Xinjiang, Gansu, and Shaanxi (Figure 3c). Similar to precipitation (Figure 3f), higher latitudes showed larger variations in DLR (Figure 3g). Overall, the three climate factors investigated in this study showed a consistently increasing trend from 1982 to 2015, providing ideal conditions for vegetation growth, which also corresponds to the conditions for the occurrence of structural overshoot.

Despite the context of such warm-wet climatic patterns, a negative trend was detected in 62.1% of the vegetated areas in SM. Furthermore, 32.5% of the vegetated areas experienced a significantly decreasing trend in SM, mostly centered in northern and central Xinjiang, southeastern Gansu, and most of Shaanxi (Figure 3d). However, most of the vegetated areas (75.9%) showed an increasing NDVI trend, of which up to 54.0% demonstrated a significantly positive trend. A rapid increase in NDVI was mainly concentrated in southern Gansu, as well as in northern and southern Shaanxi. In contrast, the areas where NDVI declined were much smaller (24.1%), primarily located near the Junggar Basin in Xinjiang, southern Qinghai, and the Hexi Corridor (Figure 3e), which is consistent with a recent study (Chen et al., 2020). It is worth noting that the areas with decreasing SM were

associated with increased precipitation and increased NDVI, suggesting that the decline in SM was not only driven by meteorological factors but also triggered by vegetation greening. Therefore, it is necessary to investigate the structural overshoot of vegetation in NWC.

To identify droughts due to vegetation overgrowth (i.e., overshoot droughts) and distinguish them from meteorological droughts, correlations between NDVI and each climate factor were calculated independently (Figure S3 in Supporting Information S1). As expected, the majority of vegetated areas exhibited positive correlations between NDVI and temperature (Figure S3a in Supporting Information S1), precipitation (Figure S3b in Supporting Information S1), and DLR (Figure S3c in Supporting Information S1), with percentages of 79.4%, 70.1%, and 79.2%, respectively, whereas negative correlations were only present in a small portion of the vegetated areas. In particular, vegetation showed a greater correlation with temperature, with a statistically significant positive correlation in 40.0% of the pixels. Moreover, 36.8% of the vegetated areas exhibited a negative relationship between NDVI and SM, and approximately 10.4% showed a significantly negative correlation, which was mainly distributed in southeastern Gansu, most of Shaanxi, and the Tarim River basin in Xinjiang (Figure S3d in Supporting Information S1). However, the NDVI in these areas exhibited a significantly upward tendency (Figure 3e), emphasizing that rapid vegetation growth may accelerate SM reduction. It is projected that the mode of warming and precipitation increase, combined with sufficient solar radiation duration, may allow vegetation to grow rapidly, which will excessively deplete SM, ultimately resulting in a shortage of water accessibility for subsequent vegetation growth, that is, the adverse lagged effect. Therefore, three meteorological factors (temperature, precipitation, and radiation (represented by DLR)) were excluded in the subsequent construction of the DLM to separate the effects of climate factors from NDVI and further detect overshoot droughts.

3.2. Identification of Droughts and Overshoot Droughts

Based on the outputs from the constructed DLM and the identification algorithm, we quantified the number and impacts of droughts and overshoot droughts in NWC from 1982 to 2015. Droughts and overshoot droughts displayed similar spatial distribution patterns (Figures 4a and 4b), approximately 34.6% of the drought events were triggered by structural overshoot. By calculating the summation of the deseasonalized detrended NDVI anomalies during drought or overshoot drought periods, and four lagged NDVI components, the impacts of droughts, overshoot droughts, and lagged components on vegetation conditions were further evaluated. The results showed overshoot droughts contributed to approximately 34.0% of the drought-induced NDVI declines, among which the lagged effects accounted for 16.7% of the vegetation degradation for these overshoot drought events. The regions with a higher occurrence probability of overshoot droughts were generally distributed in the Tarim River Basin, the Hexi Corridor, and the Loess Plateau (Figure 4b), with relatively greater impacts (Figure 4d). Overshoot droughts also occurred frequently in the Junggar Basin in northern Xinjiang but their impacts were less pronounced owing to the sparser vegetation cover and negative vegetation growth trend. A slight peak in the occurrence probability of overshoot droughts can be seen in the mid-latitudes of NWC (Figure 4g), and higher latitudes generally show more severe effects (Figure 4f). Furthermore, both droughts and overshoot droughts exhibited highly consistent temporal patterns, showing linear upward trends with increasing rates of 3,600 and 700 km² a⁻¹ from 1982 to 2015, respectively, which indicates that the intensified structural overshoot has aggravated drought impacts on the ecosystems in NWC.

To investigate the timescales at which the vegetation component contributed the most to the occurrence of overshoot droughts, four lagged timescales (i.e., sub-seasonal, seasonal, intra-annual, and inter-annual) were assessed, as depicted in Figure 5. The contribution of vegetation components to the number and impact of overshoot droughts at different lagged timescales exhibited a similar spatial distribution pattern. The sub-seasonal timescale showed the largest area distribution with percentages of 55.5% (Figure 5a) and 43.6% (Figure 5b) for the number and impact of overshoot droughts, respectively. Similarly, compared with other lagged vegetation components, the contribution of sub-seasonal vegetation components exhibited a larger proportion of overshoot droughts (43.7%) and impacts (44.5%). However, at the intra-annual timescale, the impact of vegetation overshoot was negligible. Additionally, there was a high agreement between the seasonal (25.1%) and inter-annual (25.0%) timescales in the number fraction of overshoot droughts (Figure 5a), whereas overshoot droughts induced by the seasonal timescale vegetation overgrowth resulted in greater NDVI declines, with a percentage of 30.1% compared to 22.4% (Figure 5b). Overall, NDVI lagged effects at both the sub-seasonal and seasonal timescales contributed the most to the structural overshoot droughts in NWC, implying that an earlier onset of vegetation

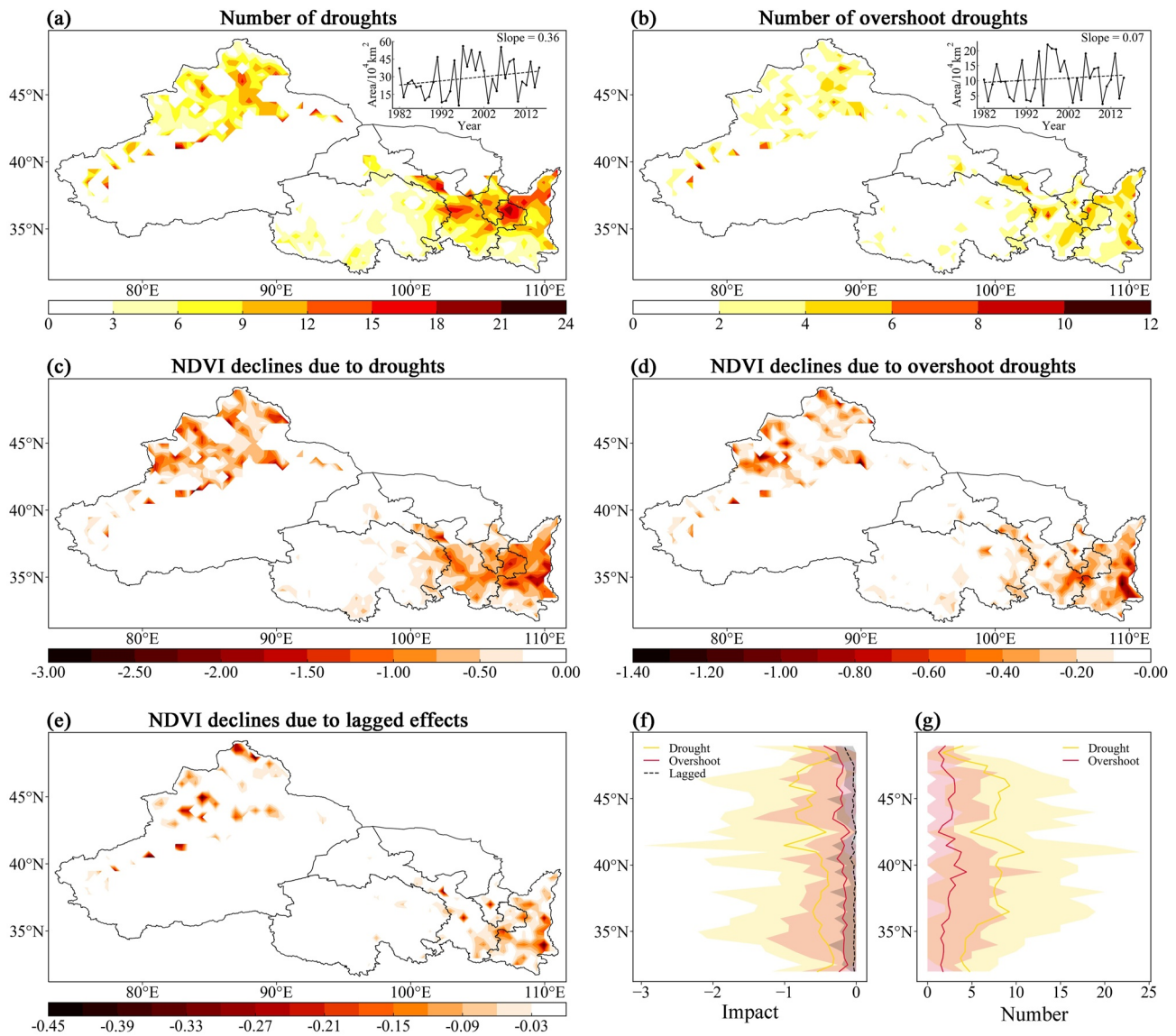


Figure 4. Spatial distributions of number and impacts of droughts and overshoot droughts. (a) The number of droughts. (b) The number of overshoot droughts. (c) Drought-induced NDVI declines. (d) NDVI declines caused by overshoot droughts. (e) NDVI declines caused by lagged vegetation effects. (f) The mean values of the impacts of droughts, overshoot droughts, and lagged vegetation at the same latitude. (g) The mean number of droughts and overshoot droughts at the same latitude. Shaded regions indicate the maximum to minimum values at the same latitude. The insets represent the inter-annual variations of the area of droughts and overshoot droughts from 1982 to 2015.

phenology driven by global warming may increase vegetation productivity in spring, which leads to greater water consumption through enhancing ET. However, the rising water limitation may ultimately result in adverse lagged effects on vegetation conditions in summer or even autumn (Jin et al., 2020), thus triggering overshoot drought (see Figure S4 in Supporting Information S1 for details).

3.3. Driving Factors of Structural Overshoot Drought

To further investigate the discrepancies in driving mechanisms between the contributions of meteorological conditions and human activities, SPEI and SWDI, representing meteorological and agricultural drought, were added to the four variables of temperature, precipitation, DLR, and NDVI in the RF model construction, to predict which factors contributed to the occurrence of overshoot drought. Using withheld and out-of-bag data, the resulting RF model can achieve an accuracy score (i.e., the proportion of correctly classified pixels)

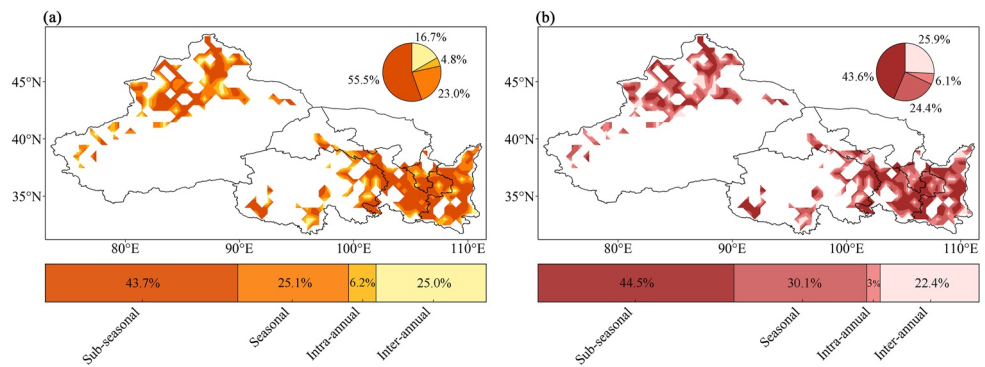


Figure 5. Overshoot droughts caused by the vegetation components at different timescales in which the maximum number (a) and impact (b) are located. The upper right pie charts indicate the proportion of pixels, and the bottom bar charts indicate the percentage of the contributions of lagged vegetation components at different timescales in terms of number and impact, respectively. Sub-seasonal, seasonal, intra-annual, and inter-annual correspond to lag 2–3, lag 4–6, lag 7–12, and lag 13–24, respectively.

of 64.3% and 65.5%, respectively, which adequately proves the validity of the RF model (Congalton, 1991). Based on the fitted RF model, the rank of VI and partial dependence of the target variable on each factor were derived.

The overshoot drought generally exhibited a non-linear response relationship with each independent driving factor. In NWC, NDVI was the primary factor causing overshoot droughts, with a VI of 0.20 (Figure 6a), and as vegetation increases, the occurrence probability of overshoot droughts increases significantly (Figure 6c). These findings are in line with our definition of structural overshoot, which states that strong vegetation growth driven by a favorable environment may consume water resources excessively and thus induce overshoot droughts later. Additionally, precipitation was more likely to trigger overshoot drought than temperature and DLR, with a VI of 0.19 (Figure 6a). This is probably attributed to the fact that the SM under arid climate is mostly low, and vegetation species in arid regions tend to respond rapidly to the changing water availability (Vicente-Serrano et al., 2013). In other words, a small amount of short-term precipitation could immediately meet the water demand of vegetation, leading it to temporarily surpass the carrying capacity of the ecosystem and increasing the occurrence probability of overshoot droughts (Figure 6b). However, an obvious turning point can be observed as precipitation reached nearly 50 mm. After this stage, the frequency of the occurrence of overshoot droughts decreased significantly

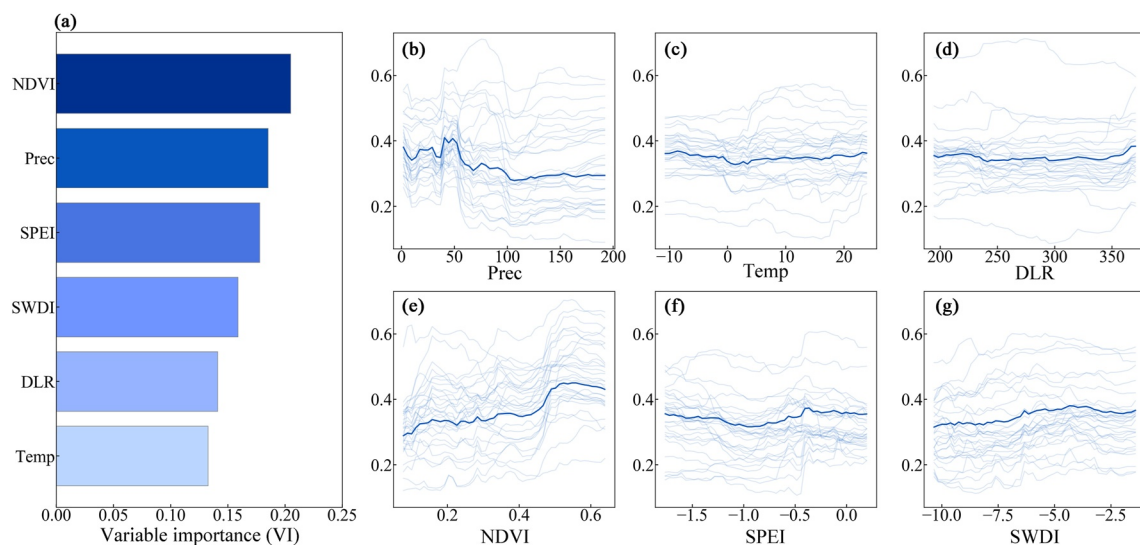


Figure 6. The rank of the variable importance (a), and the partial dependence plot corresponding to each independent variable, including Prec–precipitation (b), Temp–temperature (c), DLR (d), NDVI (e), SPEI (f), and SWDI (g). The dark blue lines indicate the average effects, and the light blue lines around them indicate 30 random incidents from the data sets.

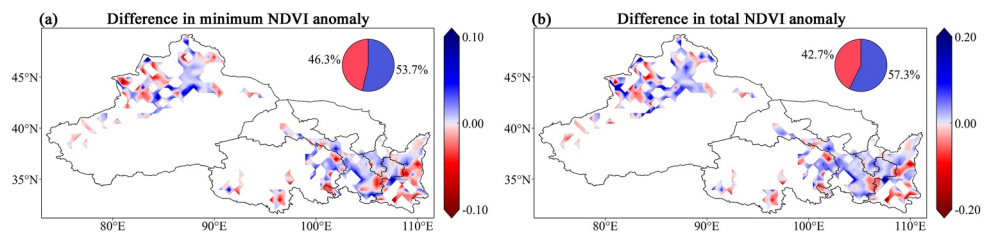


Figure 7. Differences between overshoot and non-overshoot drought periods of deseasonalized detrended NDVI anomalies in (a) minimum and (b) summation. Negative values (red) indicate a relatively greater impact of the overshoot drought, whereas positive values (blue) indicate a weaker impact.

at first and stabilized with the increase in precipitation after approximately 100 mm (Figure 6b), whereas the probability of precipitation exceeding 100 mm was relatively low in NWC, especially during drought periods.

Furthermore, the SPEI contributed to overshoot droughts more frequently than the SWDI, indicating that vegetation dynamics were responsive not only to irrigation-induced SM variations, but also to atmospheric water vapor conditions in drylands. This may be because the ecosystems of NWC are dominated by natural grasslands and woodlands, which are more susceptible to climate change (Cao et al., 2022). This study also investigated and analyzed the impact of irrigation on structural overshoot, as detailed in Section 4.2.

4. Discussion

4.1. Implications From Impacts of Overshoot and Non-Overshoot Droughts

As existing studies revealed that the Tarim River Basin in Xinjiang experienced persistent large-scale agricultural expansion from 1990 to 2015, with a significant increase in irrigated farmland (Fu, Wang, et al., 2022), which was largely driven by global warming, boosting recharging from snow and glacier retreats as well as increasing human irrigation efficiency (Fu, Wang, et al., 2022). Similarly, the Hexi Corridor, a prominent grain-producing region in China, saw an increase of approximately 14.3% in arable land area from 2000 to 2020 (Yang et al., 2023). It should be noted that both these regions had a relatively greater number of overshoot droughts. Over the past few decades, numerous ecological restoration projects have been conducted in the Loess Plateau, especially the implementation of the “Grain for Green Project” in 1999, which significantly improved vegetation coverage (Sun et al., 2015). However, the incessant growth and expansion of vegetation cover triggered structural overshoot in these areas and simultaneously caused reduced NDVI.

To evaluate discrepancies between overshoot and non-overshoot droughts, differences in the minimum and total deseasonalized detrended NDVI anomalies were calculated in this study. As shown in Figure 7, the results exhibited consistent spatial patterns between the two algorithms. However, overshoot droughts showed a greater impact on NDVI, accounting for 46.3% (Figure 7a) and 42.7% (Figure 7b) of the vegetated areas for minimum and total NDVI anomalies, respectively. These regions were primarily distributed in Shaanxi, southeastern Gansu, southern Qinghai, and parts of Xinjiang. It should be noted that overshoot droughts have already caused non-negligible consequences in the irrigated areas of Xinjiang and the Hexi Corridor, indicating that the recent agricultural expansion in NWC has worsened water scarcity (Lai et al., 2022). Moreover, the occurrence of overshoot droughts will exacerbate water limitation and accelerate vegetation deterioration, which is harmful to the ecosystem health and the growth of sustainable agriculture in fragile NWC.

According to the definition above, overshoot droughts are more likely to occur in the context of preceding favorable circumstances. Therefore, differences in temperature and precipitation between overshoot and non-overshoot drought periods were calculated to understand the potential shift in drought evolution under climate change. As shown in Figure 8, 45.7% and 40.8% of the vegetated areas correspond to the spatial distribution of the higher temperature (Figure 8a) and more sufficient precipitation (Figure 8b), respectively, which also exhibited high spatial consistency. It is worth noting that this spatial climate pattern is opposite to that of the impacts between overshoot and non-overshoot drought (Figure 7), suggesting that regions with greater non-overshoot drought effects on NDVI also possessed favorable environmental conditions. Therefore, overshoot droughts are projected to occur more frequently and have more severe effects on ecosystems. However, if high temperatures and precipitation occur asynchronously during non-overshoot drought periods, compound dry-hot extreme events may also

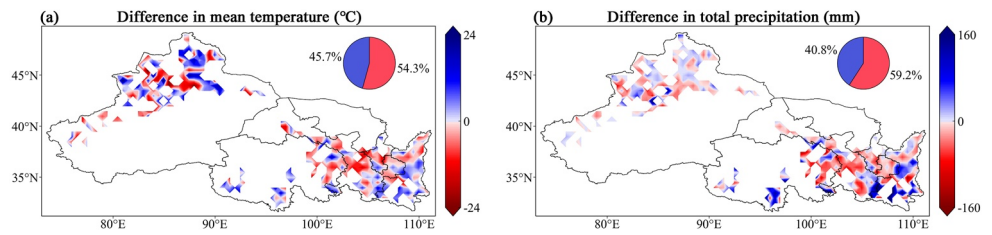


Figure 8. Differences in (a) mean temperature and (b) total precipitation between overshoot and non-overshoot drought periods. Positive values (blue) indicate that the overshoot drought period has a higher temperature or precipitation, whereas negative values (red) indicate a lower temperature or precipitation.

pose threats to ecosystems (H. W. Li et al., 2021). In this case, the simultaneous occurrence of both these events under the tendency of future climate variations could result in irreversible damage.

Over the past several decades, active afforestation projects in China have played an increasingly critical role in contributing to global vegetation greening (Zheng et al., 2021). However, a transition from greening to browning of vegetation has been discovered (Pan et al., 2018; Yin et al., 2016). Similarly, the extent of vegetation degradation has been found to increase in Xinjiang, which was previously concealed by prior natural changes and excessive vegetation growth driven by agricultural expansion (J. Du et al., 2015). Overall, our work strongly supports these documented findings, and we emphasize the importance of considering the structural overshoot of vegetation not only in NWC, but also globally.

4.2. Effects of Agricultural Irrigation on Structural Overshoot

Considering that irrigation is an important source of water supply in NWC, we chose the Xinjiang region, where irrigated agriculture is typically developing significantly, to examine the influence of irrigation water on the above outcomes. As shown in Figure 9, when the DLM was built without irrigation water as an input variable, approximately 33.8% of the drought events in Xinjiang from 1982 to 2015 were triggered by structural overshoot, whereas approximately 32.4% of drought events were identified as overshoot drought events when irrigation water (Fu, Kang, et al., 2022) was considered, showing a slight decrease in comparison to that without considering irrigation water. However, the distribution of the number of overshoot droughts along the latitude (Figure 9b) and spatially (Figures S5b and S5d in Supporting Information S1) remained similar. This is probably because the irrigated area in Xinjiang accounts for only 5% of the total area (Cai et al., 2021), whereas grassland accounts for approximately 86% of the vegetated areas (H. W. Li et al., 2021). Despite the rapid growth of irrigated agriculture in Xinjiang, its area contribution is still limited. In comparison, grasslands and woodlands are key components

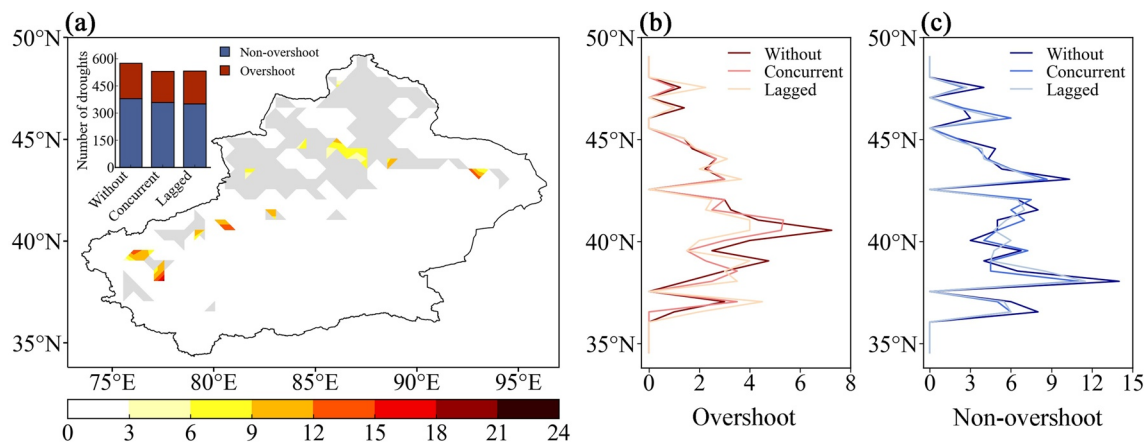


Figure 9. The spatial distribution of the number of droughts without consideration of irrigation water (a), and the distribution of the mean number of overshoot droughts (b) and non-overshoot droughts (c) along latitude. The upper left bar chart represents the number of overshoot droughts (red) and non-overshoot droughts (blue) in Xinjiang irrigated areas. The gray areas indicate the vegetated areas (mean NDVI > 0.1). Without, concurrent, and lagged indicate the inputs of DLM without irrigation water, with concurrent irrigation water, and with concurrent and previous 2 months of irrigation water, respectively, from 1982 to 2015.

of the ecosystem. In the context of warming and humidification, increasing precipitation and rising temperature, rather than human activities, may be the major contributors to vegetation recovery and the primary triggers of structural overshoot in Xinjiang. This is also consistent with the lower effect of SWDI compared to SPEI in Figure 6.

Because irrigation may potentially have a lagged effect, information on irrigation over the same period as precipitation (i.e., concurrent and previous 2 months) was also considered in this study. The results showed that 34.1% of drought events were triggered by structural overshoot (Figure 9a), which showed a slight increase compared to that without irrigation (33.8%). According to this finding, previous irrigation may also create an environment conducive to vegetation development, which could lead to vegetation overgrowth, ultimately resulting in overshoot droughts. The Xinjiang oasis region's arable land area is expanding and has the greatest greening rate of any vegetation type in the region (J. Xue et al., 2021), which is primarily driven by an increase in irrigation inputs (Cai et al., 2021). Irrigation can stabilize agricultural yields by mitigating the detrimental impacts of excess heat and low precipitation on crop growth (Troy et al., 2015). However, owing to the non-linear relationship between crop yield and irrigation water, when irrigation water consumption rises, rapid crop growth is accompanied by a significant increase in ET, thus weakening water use efficiency, and when water approaches a certain limit, crop production may be adversely changed (Sun et al., 2006). Meanwhile, owing to the impact of structural overshoot, if excessive water is irrigated in the early stage, it may also contribute to rapid crop development in the short term, which will suffer from later water stress and probably lead to a reduction in yield. Therefore, to achieve the sustainable development of agriculture and ecology, future irrigation application strategies should not only address the limitations of water use efficiency, but also be aware of the potential structural overshoot of vegetation.

4.3. Uncertainties and Limitations

The altering vegetation phenology driven by climate change that leaves a lagged effect on the subsequent vegetation growth and drought recovery has been emphasized either using remote sensors or in situ stations (Maignan et al., 2008). For example, Y. Li et al. (2023) found a negative relationship between vegetation spring phenology and drought recovery time when extreme droughts occurred in the mid-growing season of Northern Hemisphere ecosystems. Similarly, Jin et al. (2020) revealed the significant adverse lagged effects of spring greening on the subsequent summer GPP especially in dry conditions. Furthermore, Buermann et al. (2018) found higher areal fractions of adverse compared to beneficial lagged effects about vegetation productivity responses to warming springs across northern ecosystems. W. Li et al. (2022) emphasized an increasing sensitivity concerning vegetative leaf area index (LAI) to soil moisture anomalies by employing an explainable machine learning method and observations, and primarily attributed the phenomenon to inter-annual precipitation decreases. These documented studies showed great agreement with our present findings of the structural overshoot. However, there are some uncertainties and limitations in our study resulting from the model simplifications and adopted data sets.

A rising atmospheric CO₂ concentration could increase vegetation productivity and enhance water use efficiency (WUE) (Ault, 2020; Gonsamo et al., 2021). This “CO₂ fertilization effect” could increase water availability and to some extent mitigate overshoot risk. However, recent studies (F. Li et al., 2023) found a saturation of global WUE since 2001 due to increased VPD that enhanced ET, suggesting a more important role of climate factors compared to vegetative physiological changes. We further accounted for the effects of humidity or VPD on vegetation dynamics by incorporating specific humidity or VPD separately into three climate variables (i.e., temperature, precipitation, and DLR) in DLM model analysis. And results showed about 34.4% of overshoot induced drought for considering the effects of specific humidity (Figure S6 in Supporting Information S1), and about 35.2% for incorporating VPD (Figure S7 in Supporting Information S1). These results indicate an insignificant impact on our existing outcomes, highlighting the robustness of our findings.

Since NDVI is based on reflectance data, it is only responsive to changes in canopy structure and pigment concentration and might not be sensitive to the rapidly varying photosynthetic conditions of plants (Dobrowski et al., 2005). This characteristic makes the response of NDVI to water stress typically time-lagged when drought occurs and may hinder the physiological and metabolic processes of vegetation, which makes it difficult for NDVI to effectively monitor changes in photosynthetic activity (C. Li et al., 2022). As a result, it may not be sufficient to quantify vegetation dynamics by relying solely on NDVI. From these considerations, the same analysis was conducted on kNDVI, and the spatial patterns of drought and overshoot drought are consistent with

NDVI results (Figure S8 in Supporting Information S1). There is also a consistency between our results and the ones obtained from SIF, but covering a shorter period (Figure S9 in Supporting Information S1). These consensus results further support the robustness of our findings.

Additionally, some simplifications of the models and approaches were inevitable in this study. Only the effects of concurrent temperature, radiation, and precipitation from concurrent and previous 2 months, were considered in the construction of DLM. However, the lag time between vegetation and precipitation may vary across areas owing to regional heterogeneity. For example, Ning et al. (2015) discovered a 1-month time lagged effect of vegetation on precipitation in the northern Loess Plateau, whereas Ma et al. (2021) discovered that the effect of precipitation on NDVI was mostly lagged by a 1–2 months in Xinjiang. Focusing on the seasonal scale, Zhao et al. (2020) indicated that vegetation in the Loess Plateau exhibited a time lag of more than 1 month to temperature and precipitation in the spring and winter, whereas NDVI in the summer showed no lagged response to temperature but a 1-month time lag to precipitation. In addition, we did not consider the time lag in temperature and radiation, but an increase in the previous temperature or radiation that led to an increase in soil temperature may also disrupt vegetation phenology (Mulder et al., 2017). Similarly, the combined effects of temperature and precipitation over a range of timescales may also result in various changes in vegetation growth. In conclusion, it is challenging to include all probabilities because of the complicated spatiotemporal relationships between ecosystems and meteorological factors, along with the potential effects of diverse regional vegetation types and geographic elements. Additionally, higher species diversity might increase the resistance of ecosystems to drought (D. Liu et al., 2022), and different types of soil and vegetation also influence vegetation dynamics (Z. Du et al., 2017). However, these factors were not considered in the present study. Despite the uncertainties and limitations, this study revealed that vegetation greening in NWC, primarily induced by climate change, has already led to non-negligible structural overshoot. This finding is crucial for understanding the role of vegetation dynamics in the evolution of drought, which is conducive to formulating agricultural production strategies and promoting the development of measures for drought adaptation.

5. Conclusions

In this study, the structural overshoot of vegetation in the arid region of Northwest China from 1982 to 2015 was quantitatively assessed based on reanalysis and satellite remote sensing data sets. The following conclusions were drawn from the results of this study.

- (1) Temperature, precipitation, and radiation showed consistently increasing trends, which corresponded to the prerequisites for the occurrence of structural overshoot. A strong negative correlation between NDVI and SM was observed in areas where NDVI increased significantly, indicating the existence of structural overshoot.
- (2) During the past 34 years, approximately 34.6% of the drought events were induced by structural overshoot, and lagged effects explained 16.7% of the NDVI declines for these overshoot drought events. The occurrence probability of structural overshoot showed an increasing trend over time, and the vegetation component at the sub-seasonal timescale was the major contributor.
- (3) The NDVI acted as the predominant factor for the occurrence of structural overshoot, followed by precipitation, whereas the contributions of temperature and radiation were relatively small. Compared to human activities (e.g., irrigation), meteorological factors had more significant impacts on vegetation dynamics in NWC.
- (4) In regard to severity, the area extent of overshoot droughts nearly matched that of non-overshoot droughts in NWC. However, given the influence of warm-wet climatic patterns and intensified human activities, the persistent structural overshoot of vegetation is expected to escalate drought frequency and aggravate vegetation browning.

This study effectively reveals the adverse effects of structural overshoot in the ecosystem and highlights the necessity of continuously considering vegetation dynamics throughout agricultural development under future climate variation scenarios.

Data Availability Statement

The NDVI3g v1 data set is available at <http://poles.tpdc.ac.cn/en/data/9775f2b4-7370-4e5e-a537-3482c9a83d88/>. The CMFD data set is available from Yang et al. (2019). The TerraClimate data are available from Abatzoglou et al. (2018). The ERA5-Land soil moisture data are available from Muñoz Sabater (2019). The SPEI data set

is available at https://spei.csic.es/spei_database_2_6. The CSIF data set is available from Y. Zhang et al. (2018). The land cover data are available from X. Xu et al. (2018).

Acknowledgments

This research was supported by the National Natural Science Foundation of China (Grants 52079138 and 52379054), the 2115 Talent Development Program of China Agricultural University (Grant 00109019), and the National Training Program of Innovation and Entrepreneurship for Undergraduates (Grant 202210019040).

References

- Abatzoglou, J. T., Dobrowski, S. Z., Parks, S. A., & Hegewisch, K. C. (2018). TerraClimate, a high-resolution global dataset of monthly climate and climatic water balance from 1958–2015 [Dataset]. *Scientific Data*, 5(1), 1–12. <https://doi.org/10.1038/sdata.2017.191>
- Ault, T. R. (2020). On the essentials of drought in a changing climate. *Science*, 368(6488), 256–260. <https://doi.org/10.1126/science.aaz5492>
- Bastos, A., Ciais, P., Friedlingstein, P., Sitch, S., Pongratz, J., Fan, L., et al. (2020). Direct and seasonal legacy effects of the 2018 heat wave and drought on European ecosystem productivity. *Science Advances*, 6(24), eaba2724. <https://doi.org/10.1126/sciadv.aba2724>
- Belgiu, M., & Drăguț, L. (2016). Random forest in remote sensing: A review of applications and future directions. *ISPRS Journal of Photogrammetry and Remote Sensing*, 114, 24–31. <https://doi.org/10.1016/j.isprsjprs.2016.01.011>
- Breiman, L. (2001). Random forests. *Machine Learning*, 45(1), 5–32. <https://doi.org/10.1023/A:1010933404324>
- Buermann, W., Bikash, P. R., Jung, M., Burn, D. H., & Reichstein, M. (2013). Earlier springs decrease peak summer productivity in North American boreal forests. *Environmental Research Letters*, 8(2), 024027. <https://doi.org/10.1088/1748-9326/8/2/024027>
- Buermann, W., Forkel, M., O'Sullivan, M., Sitch, S., Friedlingstein, P., Haverd, V., et al. (2018). Widespread seasonal compensation effects of spring warming on northern plant productivity. *Nature*, 562(7725), 110–114. <https://doi.org/10.1038/s41586-018-0555-7>
- Cai, T., Zhang, X., Xia, F., Zhang, Z., Yin, J., & Wu, S. (2021). The process-mode-driving force of cropland expansion in arid regions of China based on the land use remote sensing monitoring data. *Remote Sensing*, 13(15), 2949. <https://doi.org/10.3390/rs13152949>
- Camps-Valls, G., Campos-Taberner, M., Moreno-Martínez, Á., Walther, S., Duveiller, G., Cescatti, A., et al. (2021). A unified vegetation index for quantifying the terrestrial biosphere. *Science Advances*, 7(9), eabc7447. <https://doi.org/10.1126/sciadv.abc7447>
- Cao, S., He, Y., Zhang, L., Chen, Y., Yang, W., Yao, S., & Sun, Q. (2021). Spatiotemporal characteristics of drought and its impact on vegetation in the vegetation region of Northwest China. *Ecological Indicators*, 133, 108420. <https://doi.org/10.1016/j.ecolind.2021.108420>
- Cao, S., Zhang, L., He, Y., Zhang, Y., Chen, Y., Yao, S., et al. (2022). Effects and contributions of meteorological drought on agricultural drought under different climatic zones and vegetation types in Northwest China. *Science of the Total Environment*, 821, 153270. <https://doi.org/10.1016/j.scitotenv.2022.153270>
- Chen, Y., Li, Z., Fan, Y., Wang, H., & Deng, H. (2015). Progress and prospects of climate change impacts on hydrology in the arid region of northwest China. *Environmental Research*, 139, 11–19. <https://doi.org/10.1016/j.envres.2014.12.029>
- Chen, Y., Yang, K., He, J., Qin, J., Shi, J., Du, J., & He, Q. (2011). Improving land surface temperature modeling for dry land of China. *Journal of Geophysical Research*, 116(D20), D20104. <https://doi.org/10.1029/2011JD015921>
- Chen, Y., Zhang, X., Fang, G., Li, Z., Wang, F., Qin, J., & Sun, F. (2020). Potential risks and challenges of climate change in the arid region of northwestern China. *Regional Sustainability*, 1(1), 20–30. <https://doi.org/10.1016/j.regsus.2020.06.003>
- Congalton, R. G. (1991). A review of assessing the accuracy of classifications of remotely sensed data. *Remote Sensing of Environment*, 37(1), 35–46. [https://doi.org/10.1016/0034-4257\(91\)90048-B](https://doi.org/10.1016/0034-4257(91)90048-B)
- Dai, A. (2013). Increasing drought under global warming in observations and models. *Nature Climate Change*, 3(1), 52–58. <https://doi.org/10.1038/nclimate1633>
- Dobrowski, S. Z., Pushnik, J. C., Zarco-Tejada, P. J., & Ustin, S. L. (2005). Simple reflectance indices track heat and water stress-induced changes in steady-state chlorophyll fluorescence at the canopy scale. *Remote Sensing of Environment*, 97(3), 403–414. <https://doi.org/10.1016/j.rse.2005.05.006>
- Du, J., Shu, J., Yin, J., Yuan, X., Jiaerheng, A., Xiong, S., et al. (2015). Analysis on spatio-temporal trends and drivers in vegetation growth during recent decades in Xinjiang, China. *International Journal of Applied Earth Observation and Geoinformation*, 38, 216–228. <https://doi.org/10.1016/j.jag.2015.01.006>
- Du, Z., Zhang, X., Xu, X., Zhang, H., Wu, Z., & Pang, J. (2017). Quantifying influences of physiographic factors on temperate dryland vegetation, Northwest China. *Scientific Reports*, 7(1), 1–9. <https://doi.org/10.1038/srep40092>
- Friedman, J. H. (2001). Greedy function approximation: A gradient boosting machine. *Annals of Statistics*, 29(5), 1189–1232. <https://doi.org/10.1214/aos/1013203451>
- Fu, J., Kang, S., Zhang, L., Li, X., Gentile, P., & Niu, J. (2022). Amplified warming induced by large-scale application of water-saving techniques. *Environmental Research Letters*, 17(3), 034018. <https://doi.org/10.1088/1748-9326/ac4b52>
- Fu, J., Wang, W., Zaitchik, B., Nie, W., Fei, E. X., Miller, S. M., & Harman, C. J. (2022). Critical role of irrigation efficiency for cropland expansion in western China arid agroecosystems. *Earth's Future*, 10(9), e2022EF002955. <https://doi.org/10.1029/2022EF002955>
- Gonsamo, A., Ciais, P., Miralles, D. G., Sitch, S., Dorigo, W., Lombardozzi, D., et al. (2021). Greening drylands despite warming consistent with carbon dioxide fertilization effect. *Global Change Biology*, 27(14), 3336–3349. <https://doi.org/10.1111/gcb.15658>
- Goulden, M. L., & Bales, R. C. (2019). California forest die-off linked to multi-year deep soil drying in 2012–2015 drought. *Nature Geoscience*, 12(8), 632–637. <https://doi.org/10.1038/s41561-019-0388-5>
- He, J., Yang, K., Tang, W., Lu, H., Qin, J., Chen, Y., & Li, X. (2020). The first high-resolution meteorological forcing dataset for land process studies over China. *Scientific Data*, 7(1), 25. <https://doi.org/10.1038/s41597-020-0369-y>
- Hersbach, H., Bell, B., Berrisford, P., Hirahara, S., Horányi, A., Muñoz-Sabater, J., et al. (2020). The ERA5 global reanalysis. *Quarterly Journal of the Royal Meteorological Society*, 146(730), 1999–2049. <https://doi.org/10.1002/qj.3803>
- Holben, B. N. (1986). Characteristics of maximum-value composite images from temporal AVHRR data. *International Journal of Remote Sensing*, 7(11), 1417–1434. <https://doi.org/10.1080/01431168608948945>
- Jamali, S., Seaquist, J., Eklundh, L., & Ardö, J. (2014). Automated mapping of vegetation trends with polynomials using NDVI imagery over the Sahel. *Remote Sensing of Environment*, 141, 79–89. <https://doi.org/10.1016/j.rse.2013.10.019>
- Jeong, S. J., Schimel, D., Frankenberg, C., Drewry, D. T., Fisher, J. B., Verma, M., et al. (2017). Application of satellite solar-induced chlorophyll fluorescence to understanding large-scale variations in vegetation phenology and function over northern high latitude forests. *Remote Sensing of Environment*, 190, 178–187. <https://doi.org/10.1016/j.rse.2016.11.021>
- Jiao, W., Wang, L., Smith, W. K., Chang, Q., Wang, H., & D'Odorico, P. (2021). Observed increasing water constraint on vegetation growth over the last three decades. *Nature Communications*, 12(1), 3777. <https://doi.org/10.1038/s41467-021-24016-9>
- Jiao, W., Wang, L., Wang, H., Lanning, M., Chang, Q., & Novick, K. A. (2022). Comprehensive quantification of the responses of ecosystem production and respiration to drought time scale, intensity and timing in humid environments: A FLUXNET synthesis. *Journal of Geophysical Research: Biogeosciences*, 127(5), e2021JG006431. <https://doi.org/10.1029/2021JG006431>

- Jiapaer, G., Liang, S., Yi, Q., & Liu, J. (2015). Vegetation dynamics and responses to recent climate change in Xinjiang using leaf area index as an indicator. *Ecological Indicators*, 58, 64–76. <https://doi.org/10.1016/j.ecolind.2015.05.036>
- Jin, J., Guo, F., Sippel, S., Zhu, Q., Wang, W., Gu, B., & Wang, Y. (2020). Concurrent and lagged effects of spring greening on seasonal carbon gain and water loss across the Northern Hemisphere. *International Journal of Biometeorology*, 64(8), 1343–1354. <https://doi.org/10.1007/s00484-020-01913-0>
- Jump, A. S., Ruiz-Benito, P., Greenwood, S., Allen, C. D., Kitzberger, T., Fensham, R., et al. (2017). Structural overshoot of tree growth with climate variability and the global spectrum of drought-induced forest dieback. *Global Change Biology*, 23(9), 3742–3757. <https://doi.org/10.1111/gcb.13636>
- Kang, S., Kimball, J. S., & Running, S. W. (2006). Simulating effects of fire disturbance and climate change on boreal forest productivity and evapotranspiration. *Science of the Total Environment*, 362(1–3), 85–102. <https://doi.org/10.1016/j.scitotenv.2005.11.014>
- Kusch, E., Davy, R., & Seddon, A. W. R. (2022). Vegetation-memory effects and their association with vegetation resilience in global drylands. *Journal of Ecology*, 110(7), 1561–1574. <https://doi.org/10.1111/1365-2745.13891>
- Lai, J., Li, Y., Chen, J., Niu, G. Y., Lin, P., Li, Q., et al. (2022). Massive crop expansion threatens agriculture and water sustainability in north-western China. *Environmental Research Letters*, 17(3), 034003. <https://doi.org/10.1088/1748-9326/ac46e8>
- Lawrence, R. L., Wood, S. D., & Sheley, R. L. (2006). Mapping invasive plants using hyperspectral imagery and Breiman Cutler classifications (RandomForest). *Remote Sensing of Environment*, 100(3), 356–362. <https://doi.org/10.1016/j.rse.2005.10.014>
- Li, C., Peng, L., Zhou, M., Wei, Y., Liu, L., Li, L., et al. (2022). SIF-based GPP is a useful index for assessing impacts of drought on vegetation: An example of a mega-drought in Yunnan Province, China. *Remote Sensing*, 14(6), 1509. <https://doi.org/10.3390/rs14061509>
- Li, F., Xiao, J., Chen, J., Ballantyne, A., Jin, K., Li, B., et al. (2023). Global water use efficiency saturation due to increased vapor pressure deficit. *Science*, 381(6658), 672–677. <https://doi.org/10.1126/science.adf5041>
- Li, H. W., Li, Y. P., Huang, G. H., & Sun, J. (2021). Quantifying effects of compound dry-hot extremes on vegetation in Xinjiang (China) using a vine-copula conditional probability model. *Agricultural and Forest Meteorology*, 311, 108658. <https://doi.org/10.1016/j.agrformet.2021.108658>
- Li, W., Migliavacca, M., Forkel, M., Denissen, J. M., Reichstein, M., Yang, H., et al. (2022). Widespread increasing vegetation sensitivity to soil moisture. *Nature Communications*, 13(1), 3959. <https://doi.org/10.1038/s41467-022-31667-9>
- Li, Y., Zhang, W., Schwalm, C. R., Gentine, P., Smith, W. K., Ciais, P., et al. (2023). Widespread spring phenology effects on drought recovery of Northern Hemisphere ecosystems. *Nature Climate Change*, 13(2), 182–188. <https://doi.org/10.1038/s41558-022-01584-2>
- Lian, X., Piao, S., Chen, A., Huntingford, C., Fu, B., Li, L. Z. X., et al. (2021). Multifaceted characteristics of dryland aridity changes in a warming world. *Nature Reviews Earth & Environment*, 2(4), 232–250. <https://doi.org/10.1038/s43017-021-00144-0>
- Lian, X., Piao, S., Li, L. Z. X., Li, Y., Huntingford, C., Ciais, P., et al. (2020). Summer soil drying exacerbated by earlier spring greening of northern vegetation. *Science Advances*, 6(1), eaax0255. <https://doi.org/10.1126/sciadv.aax0255>
- Liang, P., & Yang, X. (2016). Landscape spatial patterns in the Maowusu (Mu Us) Sandy Land, northern China and their impact factors. *Catena*, 145, 321–333. <https://doi.org/10.1016/j.catena.2016.06.023>
- Liu, D., Wang, T., Peñuelas, J., & Piao, S. (2022). Drought resistance enhanced by tree species diversity in global forests. *Nature Geoscience*, 15(10), 800–804. <https://doi.org/10.1038/s41561-022-01026-w>
- Liu, Y., Kumar, M., Katul, G. G., & Porporato, A. (2019). Reduced resilience as an early warning signal of forest mortality. *Nature Climate Change*, 9(11), 880–885. <https://doi.org/10.1038/s41558-019-0583-9>
- Liu, Y., Li, Z., Chen, Y., Li, Y., Li, H., Xia, Q., & Kayumba, P. M. (2022). Evaluation of consistency among three NDVI products applied to High Mountain Asia in 2000–2015. *Remote Sensing of Environment*, 269, 112821. <https://doi.org/10.1016/j.rse.2021.112821>
- Ma, Y. J., Shi, F. Z., Hu, X., & Li, X. Y. (2021). Climatic constraints to monthly vegetation dynamics in desert areas over the silk road economic belt. *Remote Sensing*, 13(5), 995. <https://doi.org/10.3390/rs13050995>
- Maignan, F., Bréon, F. M., Bacour, C., Demarty, J., & Poirson, A. (2008). Interannual vegetation phenology estimates from global AVHRR measurements: Comparison with in situ data and applications. *Remote Sensing of Environment*, 112(2), 496–505. <https://doi.org/10.1016/j.rse.2007.05.011>
- Marshall, M., Okuto, E., Kang, Y., Opiyo, E., & Ahmed, M. (2016). Global assessment of vegetation index and phenology lab (VIP) and global inventory modeling and mapping studies (GIMMS) version 3 products. *Biogeosciences*, 13(3), 625–639. <https://doi.org/10.5194/bg-13-625-2016>
- Martínez-Fernández, J., González-Zamora, A., Sánchez, N., & Gumuzzio, A. (2015). A soil water based index as a suitable agricultural drought indicator. *Journal of Hydrology*, 522, 265–273. <https://doi.org/10.1016/j.jhydrol.2014.12.051>
- Mei, L., Bao, G., Tong, S., Yin, S., Bao, Y., Jiang, K., et al. (2021). Elevation-dependent response of spring phenology to climate and its legacy effect on vegetation growth in the mountains of northwest Mongolia. *Ecological Indicators*, 126, 107640. <https://doi.org/10.1016/j.ecolind.2021.107640>
- Mo, K., Chen, Q., Chen, C., Zhang, J., Wang, L., & Bao, Z. (2019). Spatiotemporal variation of correlation between vegetation cover and precipitation in an arid mountain-oasis river basin in northwest China. *Journal of Hydrology*, 574, 138–147. <https://doi.org/10.1016/j.jhydrol.2019.04.044>
- Mulder, C. P. H., Iles, D. T., & Rockwell, R. F. (2017). Increased variance in temperature and lag effects alter phenological responses to rapid warming in a subarctic plant community. *Global Change Biology*, 23(2), 801–814. <https://doi.org/10.1111/gcb.13386>
- Muñoz Sabater, J. (2019). ERA5-land monthly averaged data from 1950 to present [Dataset]. Copernicus Climate Change Service (C3S) Climate Data Store (CDS). <https://doi.org/10.24381/cds.68d2bb30>
- Nemani, R. R., Keeling, C. D., Hashimoto, H., Jolly, W. M., Piper, S. C., Tucker, C. J., et al. (2003). Climate-driven increases in global terrestrial net primary production from 1982 to 1999. *Science*, 300(5625), 1560–1563. <https://doi.org/10.1126/science.1082750>
- Ning, T., Liu, W., Lin, W., & Song, X. (2015). NDVI variation and its responses to climate change on the northern Loess Plateau of China from 1998 to 2012. *Advances in Meteorology*, 2015, 1–10. <https://doi.org/10.1155/2015/725427>
- Pan, N., Feng, X., Fu, B., Wang, S., Ji, F., & Pan, S. (2018). Increasing global vegetation browning hidden in overall vegetation greening: Insights from time-varying trends. *Remote Sensing of Environment*, 214, 59–72. <https://doi.org/10.1016/j.rse.2018.05.018>
- Peñuelas, J., Rutishauser, T., & Filella, I. (2009). Phenology feedbacks on climate change. *Science*, 324(5929), 887–888. <https://doi.org/10.1126/science.1173004>
- Piao, S., Tan, J., Chen, A., Fu, Y. H., Ciais, P., Liu, Q., et al. (2015). Leaf onset in the Northern Hemisphere triggered by daytime temperature. *Nature Communications*, 6(1), 6911. <https://doi.org/10.1038/ncomms7911>
- Pinzon, J. E., & Tucker, C. J. (2014). A non-stationary 1981–2012 AVHRR NDVI3g time series. *Remote Sensing*, 6(8), 6929–6960. <https://doi.org/10.3390/rs6086929>

- Richardson, A. D., Andy Black, T., Ciais, P., Delbart, N., Friedl, M. A., Gobron, N., et al. (2010). Influence of spring and autumn phenological transitions on forest ecosystem productivity. *Philosophical Transactions of the Royal Society B: Biological Sciences*, 365(1555), 3227–3246. <https://doi.org/10.1098/rstb.2010.0102>
- Rishmawi, K., Prince, S., & Xue, Y. (2016). Vegetation responses to climate variability in the northern arid to sub-humid zones of Sub-Saharan Africa. *Remote Sensing*, 8(11), 910. <https://doi.org/10.3390/rs8110910>
- Rodell, M., Famiglietti, J. S., Wiese, D. N., Reager, J. T., Beaudoin, H. K., Landerer, F. W., & Lo, M. H. (2018). Emerging trends in global freshwater availability. *Nature*, 557(7707), 651–659. <https://doi.org/10.1038/s41586-018-0123-1>
- Samaniego, L., Thober, S., Kumar, R., Wanders, N., Rakovec, O., Pan, M., et al. (2018). Anthropogenic warming exacerbates European soil moisture droughts. *Nature Climate Change*, 8(5), 421–426. <https://doi.org/10.1038/s41558-018-0138-5>
- Shruthi, R. B. V., Kerle, N., Jetten, V., & Stein, A. (2014). Object-based gully system prediction from medium resolution imagery using Random Forests. *Geomorphology*, 216, 283–294. <https://doi.org/10.1016/j.geomorph.2014.04.006>
- Sun, H. Y., Liu, C. M., Zhang, X. Y., Shen, Y. J., & Zhang, Y. Q. (2006). Effects of irrigation on water balance, yield and WUE of winter wheat in the North China Plain. *Agricultural Water Management*, 85(1–2), 211–218. <https://doi.org/10.1016/j.agwat.2006.04.008>
- Sun, W., Song, X., Mu, X., Gao, P., Wang, F., & Zhao, G. (2015). Spatiotemporal vegetation cover variations associated with climate change and ecological restoration in the Loess Plateau. *Agricultural and Forest Meteorology*, 209–210, 87–99. <https://doi.org/10.1016/j.agrformet.2015.05.002>
- Sun, Y., Gu, L., Wen, J., van der Tol, C., Porcar-Castell, A., Joiner, J., et al. (2023). From remotely-sensed SIF to ecosystem structure, function, and service: Part I—Harnessing theory. *Global Change Biology*, 29(11), 2926–2952. <https://doi.org/10.1111/gcb.16634>
- Tao, Z., Wang, H., Liu, Y., Xu, Y., & Dai, J. (2017). Phenological response of different vegetation types to temperature and precipitation variations in northern China during 1982–2012. *International Journal of Remote Sensing*, 38(11), 3236–3252. <https://doi.org/10.1080/01431161.2017.1292070>
- Troy, T. J., Kipgen, C., & Pal, I. (2015). The impact of climate extremes and irrigation on US crop yields. *Environmental Research Letters*, 10(5), 054013. <https://doi.org/10.1088/1748-9326/10/5/054013>
- Tucker, C. J., Fung, I. Y., Keeling, C. D., & Gammon, R. H. (1986). Relationship between atmospheric CO₂ variations and a satellite-derived vegetation index. *Nature*, 319(6050), 195–199. <https://doi.org/10.1038/319195a0>
- Vicente-Serrano, S. M., Beguería, S., & López-Moreno, J. I. (2010). A multiscalar drought index sensitive to global warming: The standardized precipitation evapotranspiration index. *Journal of Climate*, 23(7), 1696–1718. <https://doi.org/10.1175/2009JCLI2909.1>
- Vicente-Serrano, S. M., Gouveia, C., Camarero, J. J., Beguería, S., Trigo, R., López-Moreno, J. I., et al. (2013). Response of vegetation to drought time-scales across global land biomes. *Proceedings of the National Academy of Sciences of the United States of America*, 110(1), 52–57. <https://doi.org/10.1073/pnas.1207068110>
- Wang, A., & Kong, X. (2021). Regional climate model simulation of soil moisture and its application in drought reconstruction across China from 1911 to 2010. *International Journal of Climatology*, 41(S1), E1028–E1044. <https://doi.org/10.1002/joc.6748>
- Wang, H., Li, Z., Niu, Y., Li, X., Cao, L., Feng, R., et al. (2022). Evolution and climate drivers of NDVI of natural vegetation during the growing season in the arid region of northwest China. *Forests*, 13(7), 1082. <https://doi.org/10.3390/f13071082>
- Wang, L. (2023). Spring phenology alters vegetation drought recovery. *Nature Climate Change*, 13(2), 123–124. <https://doi.org/10.1038/s41558-022-01579-z>
- Wang, L., Jiao, W., MacBean, N., Rulli, M. C., Manzoni, S., Vico, G., & D'Odorico, P. (2022). Dryland productivity under a changing climate. *Nature Climate Change*, 12(11), 981–994. <https://doi.org/10.1038/s41558-022-01499-y>
- Wang, S., Zhang, Y., Ju, W., Porcar-Castell, A., Ye, S., Zhang, Z., et al. (2020). Warmer spring alleviated the impacts of 2018 European summer heatwave and drought on vegetation photosynthesis. *Agricultural and Forest Meteorology*, 295, 108195. <https://doi.org/10.1016/j.agrformet.2020.108195>
- Wei, X., Huang, Q., Huang, S., Leng, G., Qu, Y., Deng, M., et al. (2022). Assessing the feedback relationship between vegetation and soil moisture over the Loess Plateau, China. *Ecological Indicators*, 134, 108493. <https://doi.org/10.1016/j.ecolind.2021.108493>
- West, M., & Harrison, J. (2006). *Bayesian forecasting and dynamic models*. Springer Science & Business Media.
- Williams, A. P., Cook, E. R., Smerdon, J. E., Cook, B. I., Abatzoglou, J. T., Bolles, K., et al. (2020). Large contribution from anthropogenic warming to an emerging North American megadrought. *Science*, 368(6488), 314–318. <https://doi.org/10.1126/science.aaz9600>
- Wolf, S., Keenan, T. F., Fisher, J. B., Baldocchi, D. D., Desai, A. R., Richardson, A. D., et al. (2016). Warm spring reduced carbon cycle impact of the 2012 US summer drought. *Proceedings of the National Academy of Sciences of the United States of America*, 113(21), 5880–5885. <https://doi.org/10.1073/pnas.1519620113>
- Wu, C., Peng, J., Ciais, P., Peñuelas, J., Wang, H., Beguería, S., et al. (2022). Increased drought effects on the phenology of autumn leaf senescence. *Nature Climate Change*, 12(10), 943–949. <https://doi.org/10.1038/s41558-022-01464-9>
- Wu, D., Zhao, X., Liang, S., Zhou, T., Huang, K., Tang, B., & Zhao, W. (2015). Time-lag effects of global vegetation responses to climate change. *Global Change Biology*, 21(9), 3520–3531. <https://doi.org/10.1111/gcb.12945>
- Xu, H. J., Wang, X. P., Zhao, C. Y., & Yang, X. M. (2018). Diverse responses of vegetation growth to meteorological drought across climate zones and land biomes in northern China from 1981 to 2014. *Agricultural and Forest Meteorology*, 262, 1–13. <https://doi.org/10.1016/j.agrformet.2018.06.027>
- Xu, X., Liu, J., Zhang, S., Li, R., Yan, C., & Wu, S. (2018). China's multi-period land use land cover remote sensing monitoring data set (CNLUCC) [Dataset]. Resource and Environment Science and Data Center. <https://doi.org/10.12078/2018070201>
- Xue, B. L., Wang, L., Yang, K., Tian, L., Qin, J., Chen, Y., et al. (2013). Modeling the land surface water and energy cycles of a mesoscale watershed in the central Tibetan Plateau during summer with a distributed hydrological mode. *Journal of Geophysical Research: Atmospheres*, 118(16), 8857–8868. <https://doi.org/10.1002/jgrd.50696>
- Xue, J., Wang, Y., Teng, H., Wang, N., Li, D., Peng, J., et al. (2021). Dynamics of vegetation greenness and its response to climate change in Xinjiang over the past two decades. *Remote Sensing*, 13(20), 4063. <https://doi.org/10.3390/rs13204063>
- Yang, K., He, J., Tang, W., Lu, H., Qin, J., Chen, Y., et al. (2019). China meteorological forcing dataset (1979–2018) [Dataset]. A Big Earth Data Platform for Three Poles. <https://doi.org/10.11888/AtmosphericPhysics.tpe.249369.file>
- Yang, L., Feng, Q., Adamowski, J. F., Alizadeh, M. R., Yin, Z., Wen, X., & Zhu, M. (2021). The role of climate change and vegetation greening on the variation of terrestrial evapotranspiration in northwest China's Qilian Mountains. *Science of the Total Environment*, 759, 143532. <https://doi.org/10.1016/j.scitotenv.2020.143532>
- Yang, L., Feng, Q., Lu, T., Adamowski, J. F., Yin, Z., Hatami, S., et al. (2023). The response of agroecosystem water use efficiency to cropland change in northwest China's Hexi Corridor. *Agricultural Water Management*, 276, 108062. <https://doi.org/10.1016/j.agwat.2022.108062>

- Yang, X., Tang, J., Mustard, J. F., Lee, J. E., Rossini, M., Joiner, J., et al. (2015). Solar-induced chlorophyll fluorescence that correlates with canopy photosynthesis on diurnal and seasonal scales in a temperate deciduous forest. *Geophysical Research Letters*, *42*(8), 2977–2987. <https://doi.org/10.1002/2015GL063201>
- Yin, G., Hu, Z., Chen, X., & Tiyyip, T. (2016). Vegetation dynamics and its response to climate change in Central Asia. *Journal of Arid Land*, *8*(3), 375–388. <https://doi.org/10.1007/s40333-016-0043-6>
- Zeng, Z., Wu, W., Ge, Q., Li, Z., Wang, X., Zhou, Y., et al. (2021). Legacy effects of spring phenology on vegetation growth under pre-season meteorological drought in the Northern Hemisphere. *Agricultural and Forest Meteorology*, *310*, 108630. <https://doi.org/10.1016/j.agrformet.2021.108630>
- Zhang, Q., Yang, J., Duan, X., Ma, P., Lu, G., Zhu, B., et al. (2022). The eastward expansion of the climate humidification trend in north-west China and the synergistic influences on the circulation mechanism. *Climate Dynamics*, *59*(7–8), 2481–2497. <https://doi.org/10.1007/s00382-022-06221-4>
- Zhang, Q., Yang, J., Wang, W., Ma, P., Lu, G., Liu, X., et al. (2021). Climatic warming and humidification in the arid region of northwest China: Multi-scale characteristics and impacts on ecological vegetation. *Journal of Meteorological Research*, *35*(1), 113–127. <https://doi.org/10.1007/s13351-021-0105-3>
- Zhang, Y., Joiner, J., Alemohammad, S. H., Zhou, S., & Gentine, P. (2018). A global spatially contiguous solar-induced fluorescence (CSIF) dataset using neural networks [Dataset]. *Biogeosciences*, *15*(19), 5779–5800. <https://doi.org/10.5194/bg-15-5779-2018>
- Zhang, Y., Keenan, T. F., & Zhou, S. (2021). Exacerbated drought impacts on global ecosystems due to structural overshoot. *Nature Ecology & Evolution*, *5*(11), 1490–1498. <https://doi.org/10.1038/s41559-021-01551-8>
- Zhang, Z., Ju, W., Zhou, Y., & Li, X. (2022). Revisiting the cumulative effects of drought on global gross primary productivity based on new long-term series data (1982–2018). *Global Change Biology*, *28*(11), 3620–3635. <https://doi.org/10.1111/gcb.16178>
- Zhao, A., Zhang, A., Cao, S., Liu, X., Liu, J., & Cheng, D. (2018). Responses of vegetation productivity to multi-scale drought in Loess Plateau, China. *Catena*, *163*, 165–171. <https://doi.org/10.1016/j.catena.2017.12.016>
- Zhao, J., Huang, S., Huang, Q., Wang, H., Leng, G., & Fang, W. (2020). Time-lagged response of vegetation dynamics to climatic and teleconnection factors. *Catena*, *189*, 104474. <https://doi.org/10.1016/j.catena.2020.104474>
- Zheng, K., Tan, L., Sun, Y., Wu, Y., Duan, Z., Xu, Y., & Gao, C. (2021). Impacts of climate change and anthropogenic activities on vegetation change: Evidence from typical areas in China. *Ecological Indicators*, *126*, 107648. <https://doi.org/10.1016/j.ecolind.2021.107648>